ROYAL SOCIETY OPEN SCIENCE

royalsocietypublishing.org/rsos

Research

Cite this article: Miszkiewicz JJ, Godinho RM, Sohler-Snoddy AM, Pasda K, Détroit F, Mahoney P, Rathgeber T, Posth C, Uthmeier T, Barbieri A. 2026 Early development of Neanderthals revealed through virtual microanatomy. *R. Soc. Open Sci.* **13**: 260485.
https://doi.org/10.1098/rsos.260485

Received: 11 March 2026
Accepted: 4 May 2026

Subject Category:
Organismal and evolutionary biology

Subject Areas:
palaeontology, evolution

Keywords:
Homo neanderthalensis, ontogeny, micro-CT, cortical bone, fetal growth, life history, interglobular dentine

Authors for correspondence:
Justyna J. Miszkiewicz
e-mail: j.miszkiewicz@uq.edu.au
Ricardo Miguel Godinho
e-mail: rmgodinho@ualg.pt
Alvise Barbieri
e-mail: abarbieri@ualg.pt

†Equal first authors.

Supplementary material is available online at https://doi.org/10.6084/m9.figshare.c.8517014.

THE ROYAL SOCIETY PUBLISHING

Early development of Neanderthals revealed through virtual microanatomy

Justyna J. Miszkiewicz[1,2,†], Ricardo Miguel Godinho[3,†], Anne Marie Sohler-Snoddy[4], Kerstin Pasda[5], Florent Détroit[6], Patrick Mahoney[7], Thomas Rathgeber[8], Cosimo Posth[9,10], Thorsten Uthmeier[5] and Alvise Barbieri[3,11]

[1]School of Social Science, The University of Queensland, Brisbane, Queensland, Australia
[2]Earth, Life, Time Group, Naturalis Biodiversity Center, Leiden, The Netherlands
[3]Interdisciplinary Centre for Archaeology and the Evolution of Human Behaviour (ICArEHB), Universidade do Algarve, Faro, Faro District, Portugal
[4]Department of Biology, The University of North Carolina at Greensboro, Greensboro, NC, USA
[5]Institute for Pre- and Protohistory, Friedrich-Alexander-Universität Erlangen-Nürnberg, Erlangen, Germany
[6]UMR 7194 HNHP, CNRS, UPVD, Muséum National d'Histoire Naturelle, Paris, France
[7]School of Natural Sciences, University of Kent, Canterbury, UK
[8]State Museum of Natural History, Stuttgart, Germany
[9]Archaeo- and Palaeogenetics, Institute for Archaeological Sciences, and [10]Senckenberg Centre for Human Evolution and Palaeoenvironment, University of Tübingen, Tübingen, Germany
[11]Department of Art and Culture, History and Antiquity, Vrije Universiteit Amsterdam, Amsterdam, The Netherlands

JJM, 0000-0002-9769-2706; RMG, 0000-0003-0107-9577; AMS-S, 0000-0002-0516-785X; KP, 0000-0003-3016-3815; FD, 0000-0001-5208-6203; PM, 0000-0002-2715-3096; CP, 0000-0002-8206-3907; TU, 0000-0003-1265-061X; AB, 0000-0002-4246-7691

The ontogeny of Neanderthal (*Homo neanderthalensis*) perinates is poorly understood due to the paucity of juvenile skeletal remains. Here we reconstruct fetal bone growth, and explore deciduous tooth structures, in three Neanderthal juveniles (Sesselfelsgrotte, 1, 2 and 3) (90 000–50 000 years ago) from southeastern Germany using non-invasive microcomputed tomography. Sesselfelsgrotte 1 exhibited bone tissue consistent with modern human perinatal plexiform-like structures and primary osteons. Long bones showed regions of advanced growth compared with the mandible and frontal bone, which can be explained through different processes of

ossification and potentially localized faster development in Neanderthals compared with modern humans. Bone microstructure resembles that of the late third trimester of modern humans, agreeing with previous estimates based on macroscopic data. Sesselfelsgrotte 2 and 3 deciduous teeth retain hypodensities deep within the crown dentine consistent with interglobular dentine. We conclude that the fetal bone patterning is similar to modern humans with some areas of advanced growth, indicating that the growth trajectory for this Neanderthal perinate was broadly equivalent to that of modern humans. The abnormal dentine mineralization points towards a possible systemic disorder.

1. Introduction

Neanderthals (*Homo neanderthalensis*) have long captivated our curiosity because they coexisted with modern humans for at least 5 kyr [1] and are relatively well represented in the fossil record [2]. Their skeletal and dental remains have allowed palaeoanthropologists to reconstruct aspects of Neanderthal lives including lifestyle, culture, diet and environmental adaptation, and their genome has revealed inbreeding with modern humans as well as admixture with Denisovans [2–6]. The Neanderthal fossil record, however, includes limited infant remains (e.g. [7–13]), some of which have been used to establish biological similarities and differences with modern human development and the juvenile period trajectories (e.g. [14–17]).

Sesselfelsgrotte (Essing, Bavaria, Germany) is one of the richest and most unique Neanderthal sites in western Europe, preserving bones and teeth of three non-adult individuals (Sesselfelsgrotte 1 to 3) indirectly dated to between 90 and 50 ka [13,18,19]. These remains consist of one deciduous upper left second molar (Sesselfelsgrotte 2), one possible deciduous lower left second molar (Sesselfelsgrotte 3) and 12 bone fragments previously ascribed to a perinate (Sesselfelsgrotte 1) based on taxonomic determination and external bone measurements performed two decades ago [13]. In this study, we take advantage of these rare osteological and dental specimens to expand the current knowledge on Neanderthal ontogeny in relation to modern humans. We perform a comparative virtual microanatomy study using microcomputed tomography (micro-CT) scans of the skeletal remains of the Sesselfelsgrotte 1 to 3 individuals. Previous studies on immature Neanderthals have demonstrated the usefulness of this virtual approach to assess skeletal microstructure, which retains evidence of living cell activity linked to the formation and growth of bone and tooth tissues (e.g. [20–23]).

We use virtual microanatomy to describe bone formation processes for Sesselfelsgrotte 1. Comparisons are undertaken with previously published data for modern humans and other Neanderthals, including previous micro-CT scans of La Ferrassie 4bis and Le Moustier 2 Neanderthal infants. The two main aims of our study are to (i) assess whether bone microanatomy corresponds with the proposed fetal third trimester stage of development for Sesselfelsgrotte 1 and in doing so expand current knowledge of ontogenetic bone formation in Neanderthal fetuses and infants, and (ii) explore the internal microstructure of Sesselfelsgrotte 2 and 3 deciduous molars.

1.1. Bone growth and microstructure in modern human fetuses and infants aged 2 years old or younger

Human skeletal development from the fetal to birth stages is an intricate biological process (e.g. [24–31]). In this section, we summarize this development with the goal of introducing key terms that will be used in our study. We will first provide an overview of skeletal development and growth processes, followed by bone histology and microanatomy changes through these developmental milestones. We will follow the terminology outlined by Moreno *et al.* [32], referring to *in utero* stages as 'prenatal' or 'fetal', and 'perinatal' when in reference to up to two months before birth, although this also includes up to 7 days postnatally.

The human skeleton begins formation *in utero* and starts to ossify through intramembranous and endochondral processes between the seventh to eighth week of the first trimester [33]. Mesenchymal cells differentiate into bone forming osteoblasts and ossification occurs on a fetal skeletal scaffold made up of fibrous membranes and hyaline cartilage [24]. Around eight weeks *in utero*, somites (mosoderm tissue that gives rise to parts of the musculoskeletal system) disappear, and joint formation begins [34]. Ossification occurs from within primary centres on the post-cranial cartilaginous scaffold, leading to the creation of long bone shafts. This process is known as endochondral ossification [24].

Most of the skull bones form through intramembranous ossification where bone tissue is deposited directly without a pre-existing cartilaginous model [35]. As the baby grows over the three trimesters of pregnancy, bone tissue continues forming, resulting in approximately 275 bones at birth. Shafts of long bones, such as the femur, lengthen from approximately 34 mm at 16 weeks to 95.5 mm at 41 weeks [28]. By 20 weeks, the bone matrix is highly organized in terms of its mineralization [36]. Until birth, fetal and perinatal bone microstructure receives great blood supply, vascularizing bone tissue. The shafts expand in diameter, while they ossify and are modelled [28] and remodelled partly with mechanical stimulation from fetal movement and kicks [37,38]. This process is executed by osteoblasts and osteoclasts which form and resorb bone tissue either independently, changing the shape of bone (modelling), or teamed up, replacing old bone with new tissue (remodelling). Histology from modern human fetuses aged five months *in utero* (20 weeks) shows the existence of osteocytes (mature osteoblasts trapped in calcified bone matrix), osteoblasts and osteoclasts, indicating that both remodelling and modelling may start early *in utero* [39].

The extensive blood supply during rapid growth results in expansive vascularity seen in fetal bone microstructure [40]. In the first trimester, the main bone tissue type present is woven, which has a haphazard collagen orientation owing to its rapid deposition [41]. In the second trimester, woven bone still dominates in a cross-section of a long bone, but it also starts to incorporate small amounts of primary lamellar bone that appear parallel-fibred (figure 1a–c) [41]. Long bone cross-sections at this stage appear trabeculae-like, with elongated regions of bone enveloping the medullary cavity separated by large spaces (figure 1d) [42], increasing structural integrity well into the third trimester. Various anatomical studies of individual modern human bones from *in utero* autopsies have evidenced this micromorphology, including the shaft of the tibia at 4–4.5 months [41]; the femur at five months (21 + 5 weeks) (figure 1d, [42, p. 276]), the rib, tibia and humerus at five–eight months (22–32 weeks) [44,45].

Approaching the perinatal stage, primary lamellar bone, which is more organized than woven, and arranged in a characteristic manner with layers of superimposed bone, develops along with primary osteons which are layers of lamellar bone enveloping longitudinal blood canals [41]. This bone tissue is still combined with woven bone, forming a characteristic appearance that is variably referred to as 'plexiform' or 'parallel-fibred' bone (figure 1e–h) [41,46–48]. This type of bone has also been observed in modern human infants, children and teenagers, during growth spurts [47,48]. The term 'plexiform' has introduced some confusion in the literature, as this type of bone is not true plexiform as that found in other mammals, where it has a distinct brick wall-like appearance [47,48].

Postnatally, and until 2 years old, woven bone is no longer predominant as it is replaced with tissues that have better organized collagen fibres. This bone tissue type is still primary but has a lamellar structure that contains primary osteons [23,48]. Very little regions of woven bone are left by 2 years old [48]. Isolated secondary osteons, with clear cement lines, will start emerging and progressively increase in density well into adulthood. Sporadic secondary osteons were observed in those aged greater than 1 year in modern human ribs and femora [23,48]. In a recent study examining humeral microstructure prenatally to 1.5 years, Moreno *et al.* [32] noted the presence of secondary osteons at six months, but not before. An earlier study by Baltadjiev [49] discussed the existence of 'osteons' and 'Haversian canals' in the tibiae of modern human fetuses, but it was referring to primary rather than secondary osteons since no cement lines were observed. Pfeiffer [48] noted possible presence of regions of 'plexiform' bone in the ribs from archaeological 0–2-year-olds. One–2-year-olds have infrequent circumferential lamellae, which become better established after 3 years old [23].

1.2. Modern human dental growth and development

Odontogenesis is a complex process that starts as early as six weeks after fertilization with the formation of the dental laminae [50]. Deciduous tooth formation ensues in the central incisors at approximately 14–16 weeks after conception [51]. By birth, all deciduous tooth types have started mineralization, and all deciduous teeth have fully erupted by approximately 2.5 years old post birth [52,53]. Root lengths vary as the crown erupts but are typically half the length of the crown at the time of tooth eruption [54].

Dentine forms the bulk of the tooth, and it is covered by enamel on the crown and by cement on the root [55]. During dentine formation, which begins around 14 weeks of development, odontoblasts migrate apically (i.e. towards the future tip of the root) away from the basement membrane (which originates the enamel dentine junction), depositing an organic extracellular matrix known as predentine [55]. Mineralization proceeds below the predentine matrix forming front, through seeding

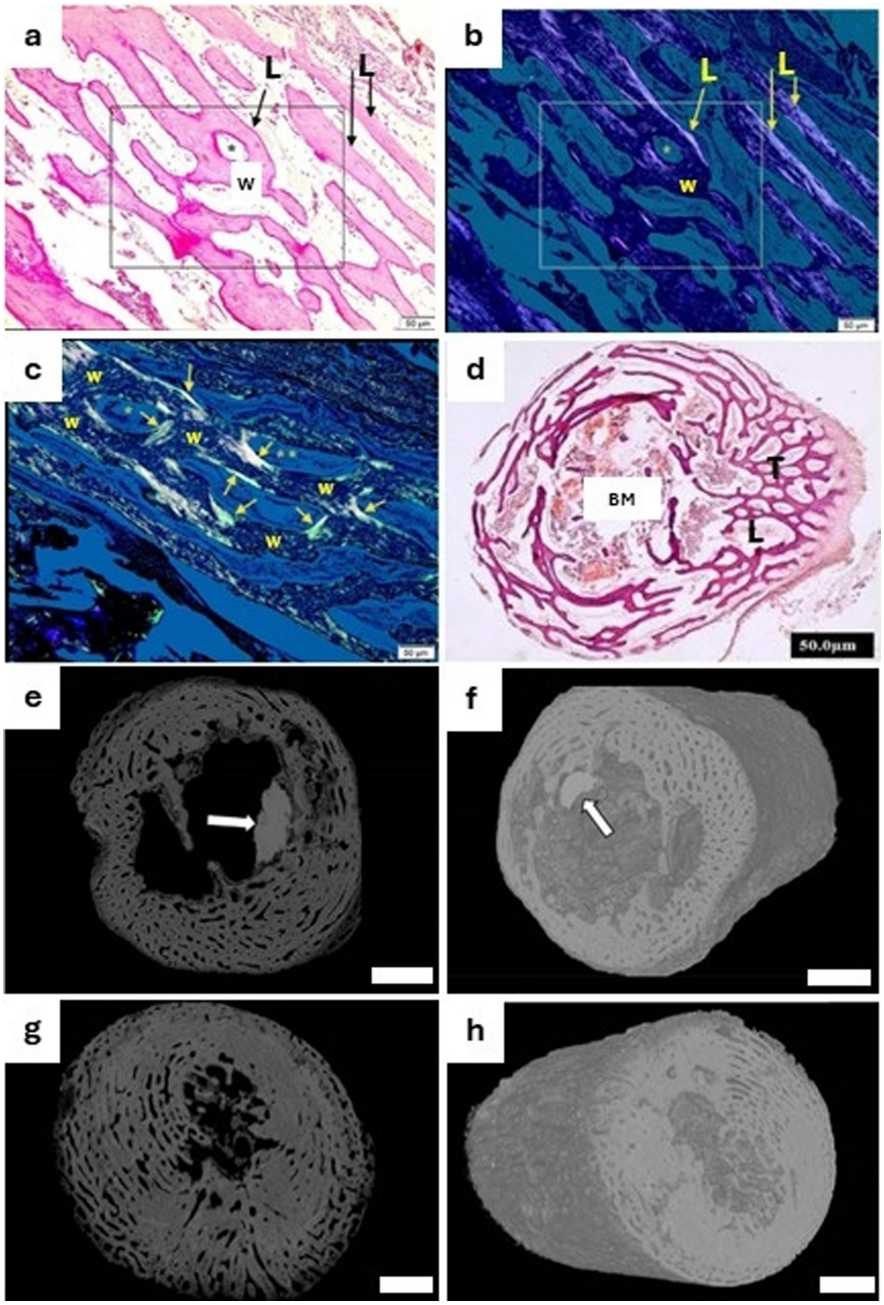

Figure 1. Histology (a–d) and micro-CT (e–h) images showing modern human bone microstructure in long bone shafts from second and third trimester stages of development. Images (a–c) are from 4–4.5 months (second trimester) tibial cortices showing trabecular-like structure of cortical bone (a–c), and presence of a combination of woven (W) and lamellar (L) bone (indicated with arrows). Scale bar in (a–c) is 50 µm. Image d shows histology in a five-month (21 + 5 weeks, second trimester) femoral diaphysis illustrating trabecular structure of cortical bone filled with bone marrow (BM). Images (e,f) are from the collection of St Mary Spital (UK) showing a diaphysis of the left femur from eight months (30–32 weeks, third trimester) showing continued trabecular, plexiform-like structure of cortical bone with increasing integrity and density. Images (g,h) are from the Stothard Place collection in eight months (30–32 weeks, third trimester), showing denser trabecular structure with plexiform-like composition. Scale bars in (e–h) are 0.9 mm. The white arrow in (e,f) is from the original publication indicating an accumulation of dense material in the medullary cavity. Images (a–c) are reprinted based on SA 4.0 open access license from [41]. Image d is reprinted from Dhawan *et al*. 2014, p. 276 [42] with permission from the European Journal of Anatomy (17 July 2025). Images (e–h) are reprinted from [43, pp. 130–131] with permission from Elsevier under license number 6160190936241.

of hydroxyapatite crystals in the predentine matrix, forming primary dentine, which is approximately 70% inorganic by weight [55]. The seeded apatite crystals grow radially, forming spherical bodies (calcospherites) that typically coalesce with other crystals, mineralizing the dentine. Occasionally,

these calcospherites fail to fuse, resulting in irregular spaces of unmineralized dentine (also known as interglobular dentine, IGD) [51]. Although small amounts of IGD are a clinically common finding, more extreme expressions of this defect may indicate a systemic disorder of mineral metabolism during growth such as rickets [56,57].

Amelogenesis (i.e. enamel formation) is initiated almost immediately after dentinogenesis has started [58]. In the secretory phase, a matrix is deposited by ameloblasts that include an organic (primarily amelogenin proteins, but also enamelin and ameloblastin) and an inorganic component (hydroxyapatite crystals). Initial enamel deposition is only partially mineralized and is ensued by maturation, which involves the removal of organic material and water by the ameloblasts and the influx of calcium and phosphate ions [51]. The hydroxyapatite crystals grow, and fully matured enamel consists of approximately 97% inorganic material by weight [55], with a pattern of ridges called perikymata on the enamel exterior. It is acellular, making it incapable of repair or regeneration following eruption.

Once the tooth crown is complete, tooth growth proceeds into the root, which is composed of dentine coated by cementum, a partially mineralized connective tissue formed by cementoblasts [58]. Root odontoblasts differentiate from dental papilla cells in a process induced by the Hertwig's epithelial root sheath, which comprises both internal and external enamel epithelium [59]. Together, these sequential and spatially coordinated processes produce the mature tooth, with distinct hard tissues exhibiting specialized histological and functional properties.

1.3. Previous fossil record for Neanderthals younger than 2 years old

The fossil record for immature Neanderthals (younger than 2 years old) is incredibly scarce. The following neonates and infants are known: 2-week-old Mezmaiskaya 1 and 1–2-year-old Mezmaiskaya 2 from Russia [7]; less than 120-day-old Le Moustier 2 from France [8–11]; 1.5–1.7-year-old Dederiyeh 1 from Syria [60]; 6–14-month-old Amud 7 from Israel [12,61]; approximately 12 days–6.5 weeks-old La Ferrassie 4bis (see details below), and 22–24-month-old Ferrassie 8 from France [8,62–64]. Only two potential Neanderthal fetuses have been so far discovered: the 8–9-month-old Sesselfelsgrotte 1 from Germany [13]; and 7-month-old La Ferrassie 5 from France [63,64]. Although La Ferrassie 4 was originally aged as a 8.5-month-old fetus [65] it was later identified in fact as being part of Le Moustier 2 [9,10] and so it is excluded as one of the existing potential fetuses of the Neanderthal record.

Ontogenetic research based on some of these specimens, while limited, has revealed that, for example, deep and short ribcages of Neanderthals were present at birth [15], their brain size at birth was probably similar to *Homo sapiens* and with comparable obstetric constraints [16,17]; but that their spatio-temporal processes underlying craniofacial transformations during early ontogeny differed from modern humans [14,66]. Further research supports that such differences in facial morphology result from contrasting growth and development processes impacting modelling and/or remodelling [67]. In the post-cranial skeleton, Sawada *et al.* [23] examined the histology of a femur midshaft cross-section in the 1.5–1.7-year-old Dederiyeh 1 Neanderthal child to find that its cortical thickness matched that of 5–6-year-old modern human (i.e. *H. sapiens*) children. Secondary osteon presence and formation patterns were similar to modern human children older than 2 years old [23]. On this basis, Sawada *et al.* [23] noted that bone development in Neanderthals might have been more advanced than in modern human children. However, the histomorphology of primary bone in the Dederiyeh 1 specimen was similar to modern human children aged 1–2 years. They concluded that Neanderthal bone growth in the early stages of ontogeny was probably different from modern humans since the Dederiyeh 1 specimen aged 1.5–1.7-year-old showed a combination of bone tissues that matched modern human children at different, mostly older, ages. The perinatal bones of the Sesselfelsgrotte 1 specimen from Germany were examined by Rathgeber [13] who estimated that they were eight months old based on comparisons with modern human and the La Ferrassie fetuses (although the bones of La Ferrassie 4 have now been reconciled with Le Moustier 2). This age estimate is on the cusp of potential birth presenting a unique opportunity to evaluate bone microstructure and Neanderthal early life ontogeny in this perinate. No study has yet examined bone microstructure in such young Neanderthal fossils, with our current knowledge in this area stemming only from bone histomorphology of the Dederiyeh Neanderthal child [13].

Previous studies of dental development that counted the number of perikymata reported that development was either comparable [68] or was advanced [69] in the teeth of Neanderthals compared with modern humans. A similar situation has been reported in histological studies that examined dental microstructures in permanent teeth, reporting that enamel growth in Neanderthals could be

faster or similar to modern humans [70–72]. Virtual microanatomical examination of deciduous teeth reported faster growth and a shorter period of development for Neanderthal incisors, canines and molars, when compared with modern humans [21]. In a recent study by Been *et al.* [61], tooth enamel histology, combined with endocranial and post-cranial skeletal examination, in Amud 7, suggested rapid growth in early life that differs from modern human infants.

Considering the limited number of Neanderthal skeletal and dental elements investigated with microanatomical methods, the remains from Sesselfelsgrotte offer a rare opportunity to further our knowledge on Neanderthal ontogeny and development.

2. Material and methods

2.1. Skeletal and dental remains and archaeological context

The Neanderthal bones and teeth in our study originate from the archaeological site of Sesselfelsgrotte (Essing, Kelheim, Bavaria, Germany). These fossils are permanently stored and curated at the Prehistoric and Protohistoric Museum of the UFG Institutes based at the Friedrich-Alexander-Universität (FAU) in Erlangen (Bavaria). Sesselfelsgrotte is a rock shelter located in the lower Altmühl Valley (Essing near Kelheim, Southeastern Germany), a region rich in Palaeolithic sites [18,73–77] (figure 2). Previous excavations at the shelter unearthed a 7 m deep sequence of limestone eboulis, in which Middle, Upper and Late Palaeolithic stays as well as historical occupations were buried [18]. The Middle Palaeolithic remains include a large faunal assemblage, microfauna remains, fire residues—including potential hearths [18], and a total of 14 human skeletal remains. These consist of the 12 potential fetal bones known as Sesselfelsgrotte 1 (skeletal elements are detailed in table 1), the fragmented buccal half of an upper left deciduous second molar labelled as Sesselfelsgrotte 2, and the fragmented approximately lingual half of a tentatively identified inferior left deciduous second molar known as Sesselfelsgrotte 3 [13]. Sesselfelsgrotte 2 was identified during the excavation of the site in 1968–1970s [18]. It was uncovered in layer M2, which exhibits a weighted thermoluminescence age of 75.9 ± 3 ka based on five dated samples (recalculated by us from original 73.2 ± 11.7 ka in Richter [78] based on excluded samples that were not indicative of Neanderthal occupation) [78, pp. 37, 39]. Contrarily, Sesselfelsgrotte 1 and 3 were identified only in the 1990s, long after their excavation [13]. Sesselfelsgrotte 3 was unearthed from layer G2, while apart from the femur and the fibula, all the skeletal remains of Sesselfelsgrotte 1 were uncovered from layer G5 in square B7. The two long bone fragments were uncovered from a collapse of the west excavation profiles of squares B7–Z7, where the G layers were exposed [18, p. 46]. Since their identification, these fetal remains have been interpreted as belonging to the same individual and from the same deposit, G5 [13]. Thermal luminescence ages from layer G4 in square A7 date the 15 cm thick sediment covering Sesselfelsgrotte 1 to 51.1 ± 10.3 ka and 57.5 ± 12.8 ka (also recalculated by us from original 56.0 ± 1.9 ka in Richter [78, p. 39]). As the deposits between G4 and M1 are undated, we conclude that the Neanderthal fetus (located in layer G5), dates either to the very end of MIS 4 or—given the fact that the thickness of the entire G-Layers-Complex measures 0.5 m only and is underlain by layers I to L with a highly arctic small mammal fauna—more probably to the very beginning of MIS 3.

Rathgeber [13] noted that almost all Sesselfelsgrotte 1 bones had short length measurements (less than 2 cm, for an overview see table 1) and appeared highly fragmented (figure 3). He assigned them to *H. neanderthalensis*, based on the archaeological attribution of the G layers. Moreover, he noted that the Sesselfelsgrotte 1 humerus and femur exhibited distinct robusticity more comparable with *H. neanderthalensis* rather than *H. sapiens*.

By comparing his measurements with data from modern human and La Ferrassie fetuses/infants, he inferred these fetal remains to be evidence of a pregnant Neanderthal female who 'lost her child in the fetal stage, around 8 months old, during her stay' at the site (translated from German [13, p. 53]). He acknowledged contention around such interpretations and arguments by others around there potentially being deliberate child burials or simple deposition of Neanderthal remains in cave sediments due to natural processes [13].

New investigations at Sesselfelsgrotte are currently led by A. Barbieri and T. Uthmeier to re-evaluate the site sequence and its assemblages, including the skeletal remains. As part of this project, the femur of Sesselfelsgrotte 1 was sampled for aDNA analysis, revealing that this is indeed a Neanderthal individual [79]. Taphonomic analyses are ongoing to clarify whether these remains were most likely buried as a cadaver by Neanderthals at the site or might have been brought to the shelter by scavengers. In the interim, a preliminary visual taphonomic examination revealed overall preservation suitable for

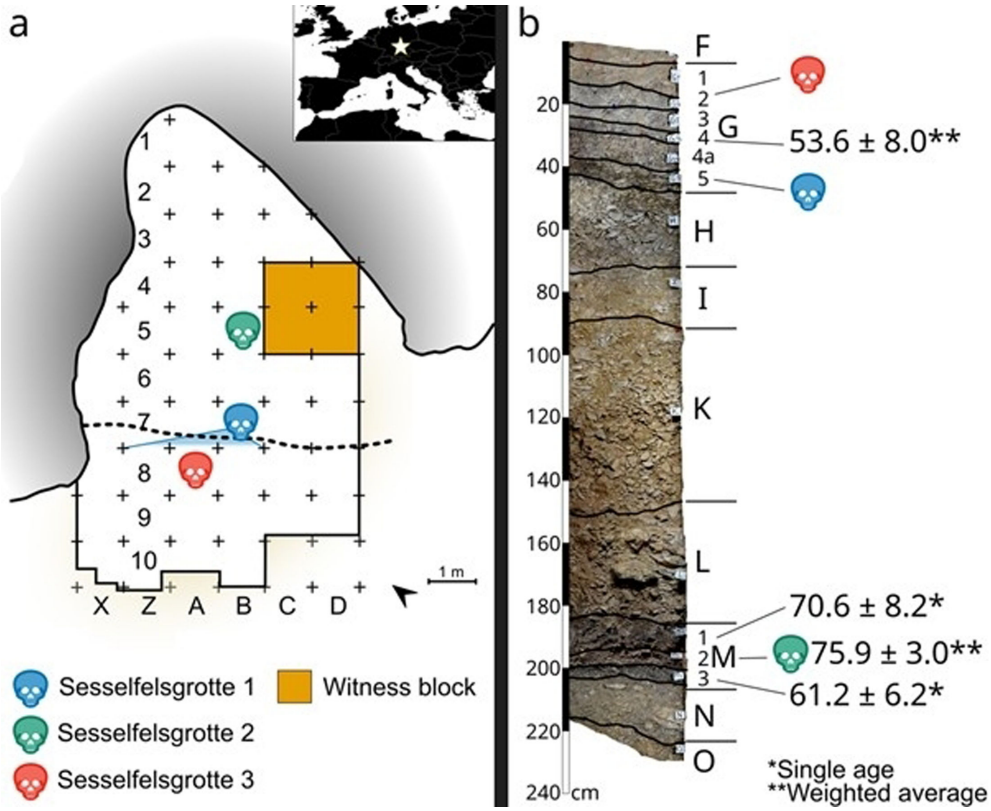

Figure 2. Stratigraphic context of skeletal and dental Neanderthal remains at Sesselfelsgrotte. (a) Planimetry of the cave in its current state, showing the location of the Neanderthal remains Sesselfelsgrotte 1 to 3. The white star in the upper right panel indicates the geographic location of the rock shelter. (b) Stratigraphic log from the witness block in square C5 displaying the vertical position of Neanderthal fossils together with available geochronological data, based on published, but recalculated, thermoluminescence results [19]. The recalculated thermoluminescence dates exclude samples that Richter [78] considered as not indicative of Neanderthal occupation.

micro-CT analyses in our study with intact internal bone structures. However, most skeletal elements showed chemical alterations of the outer bone surface that may have resulted from digestive processes. Such surface modifications are consistent with partial exposure to gastric acids and suggest that at least some bones might have been affected by carnivore activity. Only in one element, the frontale, did chemical alteration remove a portion of the outer cortex, possibly exposing inner bone structures to further alteration. Previous micro-CT scans of carnivore coprolites suggest that bone fragments ingested by carnivores, when cortical tissue is retained, can preserve intact internal microanatomical structures [80]. Thus, we expected that most of the Neanderthal remains from Sesselfelsgrotte were suitable for microanatomical study by micro-CT scanning.

2.2. Digitization, visualization and analysis

Using micro-CT, we scanned all the skeletal elements of Sesselfelsgrotte 1 to study their internal bone structure. A Nikon XT H 320 micro-CT scanner with a 0.1 mm thick copper filter at the University of Tübingen was used to digitize the bones with an isotropic spatial resolution of approximately 15–23 µm, 190 kV and 82–90 µA. The micro-CT scans of the specimens examined in this study are available open access from Morphosource [81].

Scans were visualized in 3D Slicer [82] and examined for diagenesis and bone micromorphology. Diagenesis was assessed using the Virtual Histological Index (VHI), which is a virtual complementary method to the Oxford Histological Index (OHI), both of which examine the extent of bioerosion present in bone microstructure [83]. This method relies on a visual examination of bone microstructure for preservation that ranges from excellent to poor with corresponding OHI/VHI scores from 5–0 on a 6-point scale progressing from preservation greater than 95% to less than 5% [83].

The micromorphological bone appearance in the Sesselfelsgrotte 1 individual was examined for qualitative changes in bone tissue arrangement and structure. These were: porosity/vascularity; bone

Table 1. Measurements and anatomical comments on the morphology of bones of Sesselfelsgrotte 1 (extracted from English translation of Rathgeber [13] in German). The high fragmentation of the bones precludes conclusive identification of the laterality of the fibula and of the sequence number of the ribs.

Sesselfelsgrotte 1 fossil fragments and measurements		scanned in this study
bone	**measurements from Rathgeber [13]**	
right os frontale fragment	9 mm anterior-posterior width, 10 mm high, approximately 16 mm length from the centre to the side	yes
left anterior mandibular fragment	23 mm long	yes
right vertebral arch fragment	15 mm long	yes
1/5 rib fragments, first right	18 mm long	yes
2/5 rib fragments, fourth right rib	33 mm long	yes
3/5 rib fragments, second right rib	14 mm long	no
4/5 rib fragments, shaft fragment	20 mm long	yes
5/5 rib fragments, shaft fragment	14 mm long	no
right distal humerus fragment, lower three-fifths of the diaphysis	38 mm long, distal end approximately 15 mm wide	yes
right proximal ulna fragment	40 mm long	yes
right femur fragment, proximal end of the diaphysis, and proximal two-thirds of the shaft	53 mm long	yes
right proximal fibula (shaft)	21 mm long	yes

tissue type presence and arrangement (woven, lamellar, primary, secondary, plexiform-like), presence or absence of primary osteons and/or secondary osteons [41,47,48]. We acknowledge that it is essentially not possible to identify woven and lamellar bone collagen orientation from micro-CT scans. Ground histology is appropriate for this type of analysis. Therefore, instead of providing definitive confirmation of woven bone presence, we use the term 'probably' to indicate that the bone arrangement seen is not of typical lamellar layering thus pointing to the likely existence of woven bone tissue. Our micro-CT resolution did not reach cell level details to assess osteocyte lacunae densities, which will remain undescribed here. Our study did not receive permissions to perform invasive analyses, such as ground histology, which would have otherwise offered higher resolution. The fossils could not be removed for scanning at a Synchrotron facility either as we had to limit radiation exposure to enable further sampling for aDNA analysis. With these limitations in mind, we reviewed the entirety of each scanned bone slice by slice, and here provide a summary examination of three main slices per bone taken at three equal segments. As is standard in bone microstructure research, we first describe bone microstructure in each bone on its own and then present overall patterns.

We then compare our findings to published fetal, neonatal and infant bone microstructure, where available, to check to what extent our observations were consistent with images and data published for various ages [41–43,46,48,84,85]. The comparative sample also includes micro-CT scans of the La Ferrassie 4bis and Le Moustier 2 Neanderthals, to which access was granted by the Muséum national d'Histoire naturelle (Paris). Le Moustier 2 originates from a layer which has been dated to 40.3 ± 2.6 ka by thermoluminescence [9,86] and has an estimated age-at-death of less than 120 days old [8] (the right humerus and femur identified as La Ferrassie 4 were originally osteometrically aged as 8.5 fetal months at death by Heim [64,65], but were later attributed to Le Moustier 2 based on osteometry and tooth calcification [8,9]). To the best of our knowledge, there are no dates for La Ferrassie 4bis, nor is the precise stratigraphic origin known, and there are two age-at-death estimates of 12 days post-partum [65] and 6.5 weeks post-partum [62]. Notwithstanding, dates for La Ferrassie burials have ranged from 54 ± 4 and 43 ka based on luminescence [87] to the end of the Middle Palaeolithic less than 52 ka based on more recent combined ^{14}C and optically stimulated luminescence [88].

The two deciduous teeth of two other individuals from Sesselfelsgrotte (2 and 3) were first examined macroscopically. Both teeth appear to show evidence of root resorption and severe dental wear (but see details below). These specimens were also micro-CT scanned and visualized in 3D Slicer

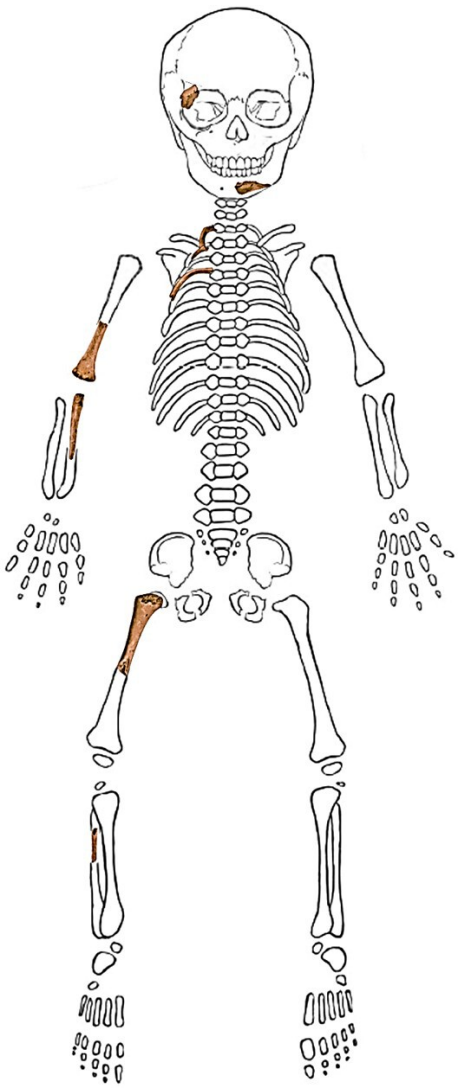

Figure 3. Combined images of the inventory of the fetal remains of Sesselfelsgrotte 1, lacking the bones of the vertebral neural arch because precise identification (i.e. which vertebra) is not conclusive. The high fragmentation of the bones also precludes conclusive identification of the laterality of the fibula and of the sequence number of the ribs.

[82] to examine their internal structures. Hypodense regions found in the dentine were highlighted manually and visualized in three dimensions to enable examination of their spatial distribution within the teeth.

3. Results and discussion

3.1. Bone

All bone slices showed overall very good preservation, which resulted in all VHI scores of greater than 4 meaning preservation greater than 85% (after [83]; electronic supplementary material, table S1). Only the vertebral specimen was assigned a VHI score of 3.5 due to localized bioerosion which was mostly located in the marrow spaces between bone spicules. We were apprehensive about assigning scores of 5 (greater than 95% preservation) because of the imperfect resolution, but it was clear that any bone diagenesis that was present in the samples was either restricted to the medullary cavity or localized to the sub-periosteum.

All bone fragments examined show bone microstructure consistent with a rapidly forming and growing immature skeleton. We group our descriptions based on developmental pathways: intramembranous ossification in the mandible and the frontal bone fragment, and then endochondral ossification

in the vertebral fragment, the rib fragments and the long bone (humerus, ulna, femur, fibula) fragments. A summary of our observations is provided in table 2.

Both the *mandible* and the *frontal* bone fragments (figure 4), which form through intramembranous ossification, showed slightly different microstructural patterns when compared with the long and other irregular bones that form through endochondral ossification. The shape of the cross-sections is irregular given the predominance of trabecular form over cortical in these bones, but clear high vascularity is still observed in both specimens both on the inferior and superior bone surfaces. Series of primary osteons were clearly seen in the mandible on the superior bone surface, with possible small areas of primary lamellar bone in the same region, but overall, both specimens were still at the plexiform-like stage of formation.

The *vertebral* fragment (figure 4) showed high vascularity throughout its thin cortex, which is consistent of both plexiform-like and trabecular-like structure. There was localized bioerosion covering the trabeculae within the internal spongy component of the vertebra, which obscures the microanatomy, but the cortical area exhibited possible small areas of primary lamellar bone. The bone tissue in the three *ribs* (figure 5) shared similar micromorphology with high vascular densities arranged in a plexiform manner and isolated primary osteons. The medullary cavity here was small in proportion to the cortical area with remnants of trabecular bone. Rib 2 showed a possible small region of primary lamellar bone on the cutaneous surface, but this was only noticeable in the rib region located towards the sternal end (see slice 3) and not in the other parts or the other ribs (see slices 1 and 2).

The long bone shafts (figure 6) all shared very similar micromorphology, with the largest of the four bones (femur and humerus) showing overall higher density of compact bone on the intra-cortical and sub-periosteal region than the ulna and the fibula. This was particularly evident on the slices viewed in the midshaft area of these bones. The *humerus* (figure 6a) fragment near the midshaft showed distinct isolated trabeculae and a proportion of bone tissue: medullary cavity nearing 1 : 1 ratio in terms of occupied space. It showed the lowest porosity (in terms of vascular spaces) compared with the femur and the ulna. There were primary osteons seen along with the remnants of plexiform-like woven bone complex spanning the entirety of the compact wall. There were also possible regions of primary lamellar bone nearer the midshaft on the postero-medial aspect. Out of all the long bones, the *ulna* (figure 6b) showed the highest vascularity of a combination of radial and transversely oriented canals of the plexiform-like pattern. At the shaft, its medullary cavity did not retain trabecular form and the compact bone layers showed only sporadic primary osteons restricted to the endosteal regions of bone, but with possible areas of primary lamellar bone on the postero-lateral aspect. Nearing the proximal end where spongy bone appeared, there were clear trabeculae present surrounded by highly vascularized thin cortex.

The *femur* (figure 6c) showed the largest cross-section compared with the other long bones with emptier medullary space than that of the humerus with a limited number of trabeculae restricted to the endosteal region. Vascularity characterized by plexiform-like arrangement was obvious on the sub-periosteal region, particularly on the antero-medial surfaces, but it transitioned into primary osteon lamellar form intra-cortically and towards the endosteal areas with localized radial canals. The shaft of the *fibula* (figure 6d) showed an oval cross-section with a well-defined medullary cavity retaining only a small number of endosteally peripheral trabeculae. The cortical bone was well vascularized, with primary osteons and small regions of primary lamellar bone on the antero-lateral surfaces and areas of plexiform-like structure on the postero-medial aspect.

Once compared (summary in table 3) with the information and images available in the literature and anatomical sources [23,41,43,85], and scans for the less than 6.5 weeks post-partum La Ferrassie 4bis and less than 120 days old Le Moustier 2 (figure 7), the highest similarity in the microanatomical appearance was with the femoral midshaft micro-CT slices from Romano-British archaeological pre-term individuals [43] aged 30–36 weeks (some shown in figure 1e–h). Comparisons with femoral and humeral shaft micro-CT slices from La Ferrassie 4bis and Le Moustier 2 did not quite agree, with Le Moustier 2 showing stronger compaction of the cortical walls, while La Ferrassie 4bis showing intense vascularity. Sesselfelsgrotte 1 scans had a mix of these features. However, in La Ferrassie 4bis, the femur and humerus were highly impacted by bioerosion, so it is difficult to comment further on vascularity structures. The Le Moustier 2 femur and humerus also showed some bioerosion in the cortical bone, obscuring microanatomical structures, but the compactness of bone and well-defined cortical and trabecular spaces indicated a relatively older individual than Sesselfelsgrotte 1.

Overall, the micro-CT scans of bone microanatomy of fragments of the femur, humerus, ulna, fibula, three ribs, mandible, vertebra and frontal bone of Sesselfelsgrotte 1 revealed skeletal tissue structure partly consistent with late third trimester gestation in *H. sapiens*, but showing regions of

Table 2. Summary of bone microstructural changes observed in the bones of Sesselfelsgrotte 1.

bone markers	porosity/ vascularity	bone tissue with plexiform-like arrangement	cortical bone has trabecular-like structure	bone tissue with primary lamellar arrangement	woven bone	primary osteons	secondary osteons
right frontal bone							
slice 1	high	yes	yes	no	probably	yes	no
slice 2	high	yes	yes	no	probably	yes	no
slice 3	high	yes	yes	no	probably	yes	no
left mandible							
slice 1	high	yes	possibly	possibly	probably	yes	no
slice 2	high	yes	yes	possibly	probably	yes	no
slice 3	high	yes	yes	no	probably	yes	no
vertebra							
slice 1	high	yes	yes	no	probably	yes	no
slice 2	high	yes	partly	possibly	probably	yes	no
slice 3	high	yes	partly	possibly	probably	yes	no
rib 1							
slice 1	high	yes	no	no	probably	yes	no
slice 2	high with low region	yes	no	no	probably	yes	no
slice 3	high with low region	yes	no	no	probably	yes	no
rib 2							
slice 1	high	yes	no	no	probably	yes	no
slice 2	high	yes	no	no	probably	yes	no
slice 3	high with low region	yes	no	possibly	probably	yes	no
rib 4							
slice 1	high with low region	yes	no	no	probably	yes	no

(*Continued.*)

Table 2. (*Continued.*)

bone markers	porosity/vascularity	bone tissue with plexiform-like arrangement	cortical bone has trabecular-like structure	bone tissue with primary lamellar arrangement	woven bone	primary osteons	secondary osteons
slice 2	high with low region	yes	no	no	probably	yes	no
slice 3	high with low region	yes	no	no	probably	yes	no
right humerus							
slice 1	low	yes	no	possibly	probably	yes	no
slice 2	low with high region	yes	no	possibly	probably	yes	no
slice 3	high	yes	yes	no	probably	yes	no
right ulna							
slice 1	high	yes	yes	no	probably	yes	no
slice 2	high with low region	yes	no	possibly	probably	yes	no
slice 3	high with low region	yes	no	possibly	probably	yes	no
right femur							
slice 1	high	yes	yes	no	probably	yes	no
slice 2	low	yes	no	possibly	probably	yes	no
slice 3	low	yes	no	possibly	probably	yes	no
right fibula							
slice 1	high	yes	no	no	probably	yes	no
slice 2	high with low regions	yes	no	possibly	probably	yes	no
slice 3	high with low regions	yes	no	possibly	probably	yes	no

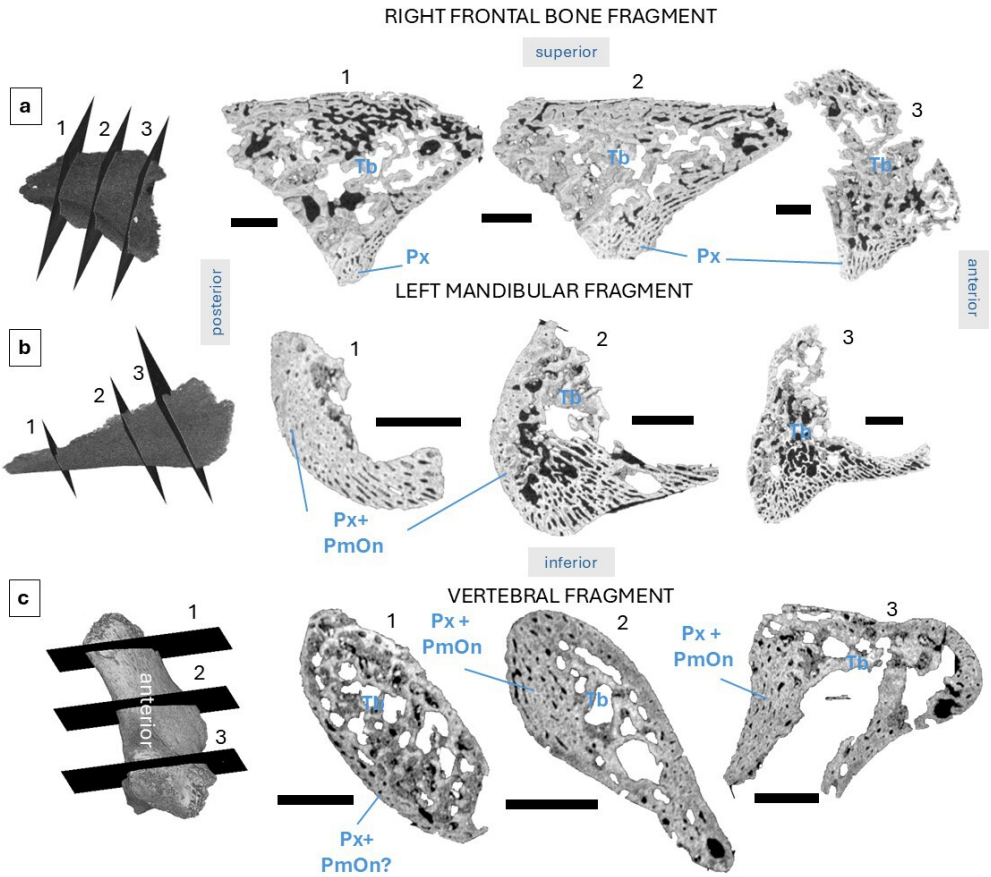

Figure 4. Bone microanatomy in Sesselfelsgrotte 1 visualized in three slices per bone fragment: right frontal bone fragment (a), left mandibular fragment (b), and vertebral fragment (c, most likely anterior view). Scale bars are 10 mm. Labels are in representative regions only indicating plexiform-style bone (Px), primary osteons (PmOn), combination of Px and PmOn (Px + PmOn), trabeculae (Tb) and possible beginning of compaction (Cm?).

advanced bone formation that is typically seen in modern human neonates. Our findings support the age estimates based on macroscopic measurements presented by Rathgeber [13] around the eighth fetal month mark. Our analysis also brings new information about Neanderthal *in utero* development of the skeleton, showing remarkable similarities to modern human fetal bone microstructure this late in the final trimester of pregnancy. This supports what has been previously proposed using Neanderthal and modern human long bone microstructure around both taxa sharing similar developmental infant trajectories up until approximately 1–2 years of age after which modern humans depart from Neanderthal type bone microstructure [23].

Our examination of bone microstructure agreed with fetal bone formation and growth in modern humans. The very characteristic plexiform-like bone structures and probable woven bone seen in all the Sesselfelsgrotte 1 bones indicate clearly that they belonged to an individual whose skeleton had not yet been exposed to significant mechanical and temporal factors that would otherwise stimulate the formation of more mature bone tissues. We refer to this tissue type as plexiform-like because it is thought that modern humans do not deposit plexiform tissues as defined in other larger mammals that have a rapid juvenile growth [47,48]. In those mammals, plexiform bone takes a distinct brick-wall pattern of superimposed layers of bone. In modern human fetal bone, this tissue is more disorganized with irregular vascular spaces which can orient themselves in many directions. The presence of this bone tissue in combination with primary osteons is evidence that bone is experiencing rapid growth, which is expected for fetuses. While plexiform-like bone tissue has been previously documented in older modern human children who undergo growth spurts [89], the macroscopic measurements and comparative analyses undertaken by [13] would rule out a much older child. Further, none of the Sesselfelsgrotte 1 bones showed any obvious primary lamellar bone arranged in clear successive layers to begin forming circumferential lamellar bone, both of which would indicate the slowing down of bone formation and deposition of bone that is better organized than woven and plexiform-like. Sawada *et al.* [23] noted a lack of circumferential lamellae in the Dederiyeh 1 Neanderthal child at 1.5–1.7

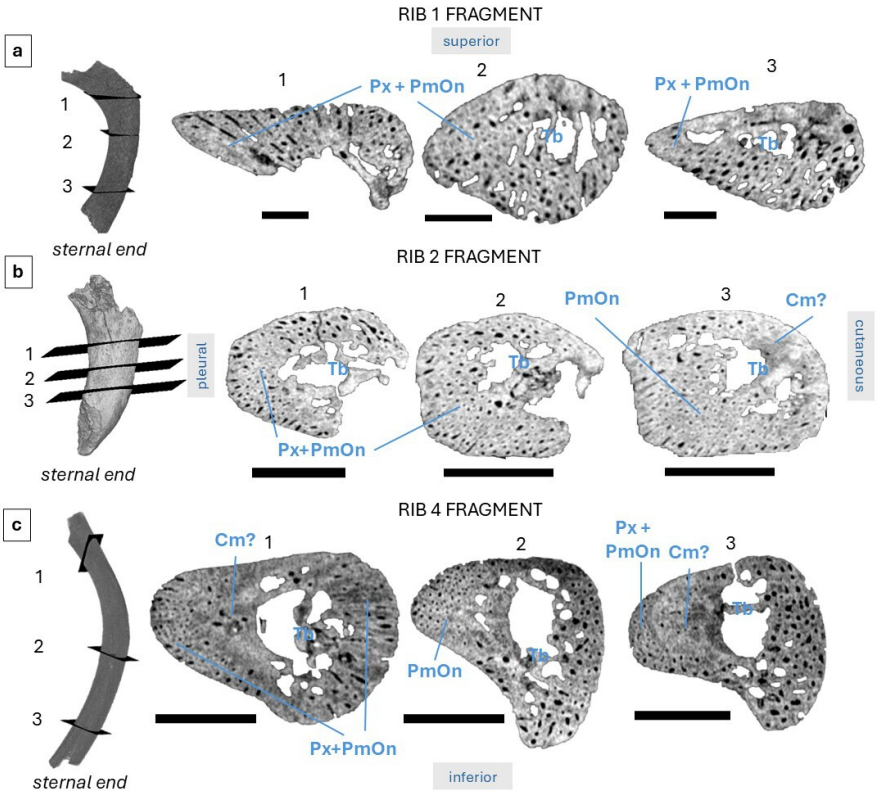

Figure 5. Bone microanatomy in Sesselfelsgrotte 1 visualized in three slices per rib fragment. Scale bars in panel a are 5 mm, while panels b–c show scale bars that measure 10 mm. Labels are in representative regions only indicating plexiform-style bone (Px), primary osteons (PmOn), combination of Px and PmOn (Px + PmOn), trabeculae (Tb) and possible beginning of compaction (Cm?).

years, but there was presence of secondary and primary osteons. We identified primary osteons, but no secondary osteons.

The overall complex of bone tissues in our specimens was clearly a combination of probably woven, plexiform-like and some primary osteons, with regions of the humerus and femur showing progression towards increased compactness and more structured organization. These areas may indicate a slight advancement in bone growth that would be consistent with conclusions made by Sawada *et al.* [23] that Neanderthal cortical bone histology (at least in the femur) has features different from modern humans despite similarities in primary bone in the first 1–2 years. If that is the case, we of course cannot confirm the underlying causes of possible bone growth advancement in the Sesselfelsgrotte 1 Neanderthal. Neanderthal skeletal robusticity both at the juvenile and adult stages has been consistently linked to climate adaptation, lifestyles of various physical demands, varied diets and faster development than that of modern humans [90,91]. Considering the subject of our study is perinatal bones, we can only propose an alternative or a combination of factors such as dietary, maternal and genetic, since it is known that these factors can determine the speed with which the fetal skeleton forms [92]. While the biomechanics of a Neanderthal fetus are essentially impossible to study, the existing body of knowledge about modern human fetal movement (e.g. reviewed in [93]) and morphological similarities between Neanderthals and modern humans, suggest that Neanderthals might have experienced similar ranges of fetal movement yielding *in utero* mechanical stimulation (e.g. twitching; stretching; full body, limb, head/neck/jaw movements) supporting internal bone formation. The possible areas of the beginning of compactness in the femur and the humerus in our specimens could point to these fetal movements being correspondingly strong to Neanderthal robusticity that develops in later stages of ontogeny. While prior Neanderthal obstetric research, where virtual reconstructions of brain size at birth in Russian and Syrian specimens, and the pelvic canal shape in the adult Tabun female, indicated similarities to modern humans with a somewhat more primitive Neanderthal birth mechanism [17,94], our findings may point to some increases in Neanderthal mechanical *in utero* stimulation driving microstructural bone deposition preceding postnatal modelling of the bone exterior. These bone regions of possibly more advanced than modern human growth

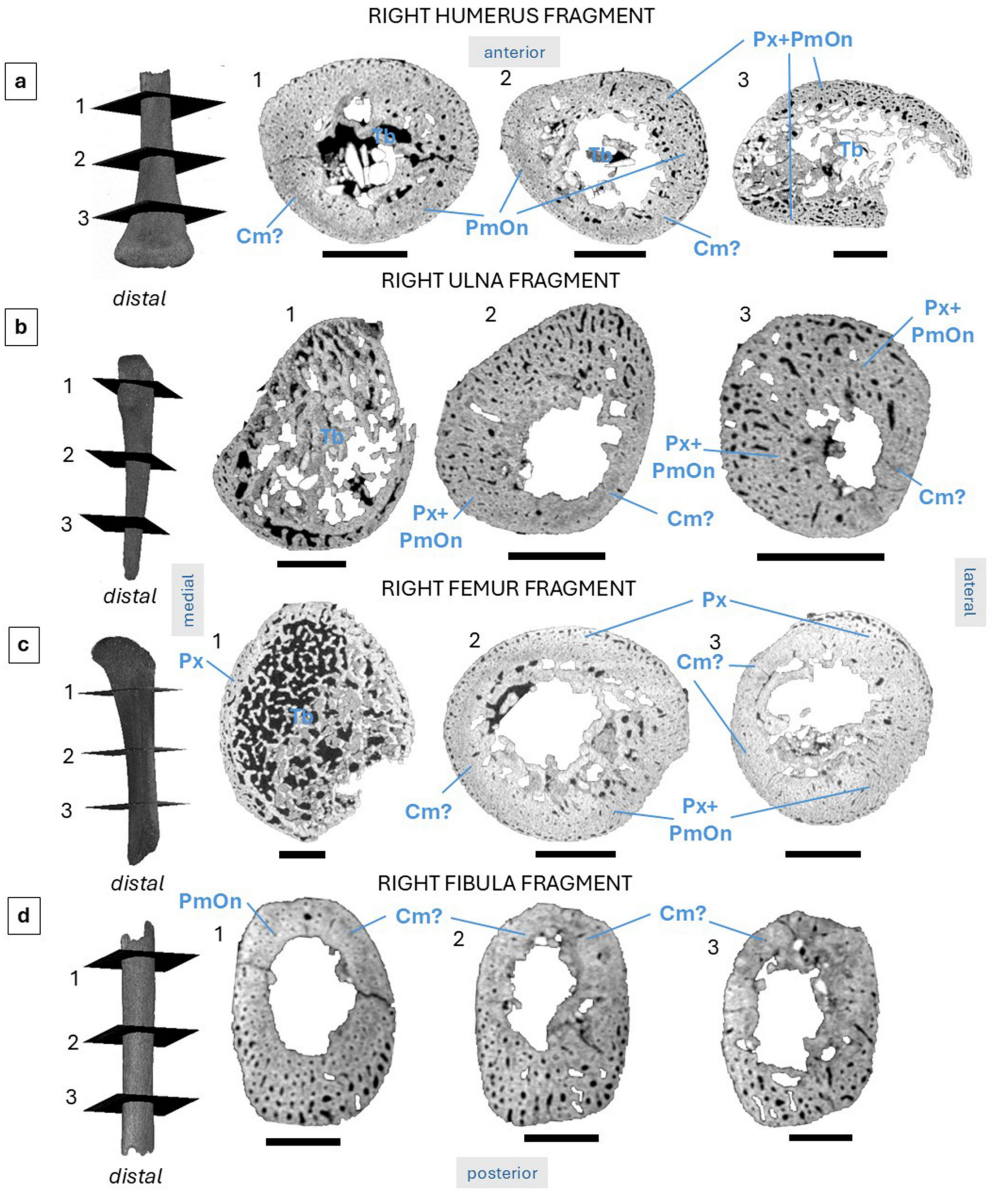

Figure 6. Bone microanatomy in Sesselfelsgrotte 1 visualized in three slices per bone fragment: right humerus fragment (a, posterior view), right ulna fragment (b, posterior view), right femur fragment (c, posterior view) and right fibula fragment (d, posterior view). Scale bars in panels (a–c) are 10 mm, while panel b shows scale bars of 5 mm length. Labels are in representative regions only indicating plexiform-style bone (Px), primary osteons (PmOn), combination of Px and PmOn (Px+PmOn), trabeculae (Tb) and possible beginning of compaction (Cm?).

would also agree with the notion presented recently in Been *et al.* [61] who indicate rapid growth strategies in Amud 7 aged 4–16 months.

Having said this, our observations of bone microstructure are limited by the imperfect resolution of the micro-CT scans, which most obviously hindered our ability to evaluate cell-level information at the osteocyte lacuna level, but we avoided invasive (such as ground histology) and radiation analyses due to their destructive nature. While we treat here micro-CT as a non-invasive method, we acknowledge there has been a discussion in the literature around the level of destructiveness of micro-CT, concluding that it is not strictly non-destructive as some damage to DNA and ancient proteins occurs following repeated scans [95–97]. These other more destructive methodological approaches could have aided in gathering more data, particularly clarifying any more localized bioerosion and allowing us to conduct quantitative analyses, such as estimating primary osteon counts and densities, in addition to clarifying collagen fibre morphology in different tissue types. The fragmentary preservation of the fossils also means we cannot comment on bone formation in other bones or the remaining parts of bones.

Table 3. Summary of our observations consistent with information and images available in the literature.

bone/specimen	reference	age	Sesselfelsgrotte 1 comparisons (younger/older/similar)		
			rib	humerus	femur
modern human fetal femur midshaft histology	[85]	14–26 weeks	—	—	older
modern human fetal femur microanatomy (IS6)	[43]	34–36 weeks	—	—	similar
modern human fetal femur microanatomy (IS7)	[43]	30–32 weeks	—	—	similar, potentially slightly older
modern human fetal femur microanatomy (IS10)	[43]	30–32 weeks	—	—	similar, potentially slightly older
Neanderthal femur midshaft histology	[23]	approximately 2 years old	—	—	younger
modern human femur midshaft histology	[23]	approximately 1 year old	—	—	younger
modern human femoral and humeral fetal parallel-fibred lamellar bone deposited on fetal woven bone cores	[41]	approximately 17.4 to 19.6 gestational weeks	—	older	older
modern human juvenile rib	[48]	0–1 years	younger	—	—
modern human juvenile humerus	[84]	0–1.9 years	—	younger	—
modern human fetal femur	[42]	21+5 weeks	—	—	older
modern human neonatal femur	[46]	less than 1 year	—	—	younger
La Ferrassie 4bis	figure 7	less than 6.5 postnatal weeks	—	older	some similarities
Le Moustier 2	figure 7	less than17.2 weeks	—	younger	younger

Another large limiting factor in our study is the bioerosion seen in the comparative Neanderthal fetal bone microanatomy. This means all of our conclusions are based on comparisons with modern humans and limited information for Neanderthals, such as ground histology of the Dederiyeh 1 child [23] and imperfect microanatomical micro-CT scans. Deciduous tooth crowns could have also confirmed whether this Neanderthal was in fact born and estimate age-at-death by using the neonatal line and enamel incremental lines [70], but regrettably there are no teeth preserved in Sesselfelsgrotte 1. Further, while acknowledging the complexities of histotaphonomic experiments and interpretations, the excellent preservation in Sesselfelsgrotte bones compared with the obvious bioerosion in the La Ferrassie 4bis and some bioerosion in Le Moustier 2 scans, points to a hypothesis of birth circumstances. Booth [98] and Booth *et al.* [43] associate many human infants in the archaeological record showing no bioerosion with stillbirth or death shortly after birth. Future research in this area should aim to undertake multi-methodological approaches at higher resolution to further contribute to our current understanding of Neanderthal fetal bone microstructure. Finally, it must be stated that using modern humans as a reference point for understanding differences and similarities in perinatal bone development between modern humans and Neanderthals, with the limited samples at hand, risks circularity in our arguments. This is apparent from Rathgeber's [13] eight month age estimate of Sesselfelsgrotte 1, which was obtained using modern human and La Ferrassie and Le Moustier fetuses as reference points. Thus, we cannot uncover the pace or speed of developmental variation across Neanderthals and humans, but offer a simple comparative perspective.

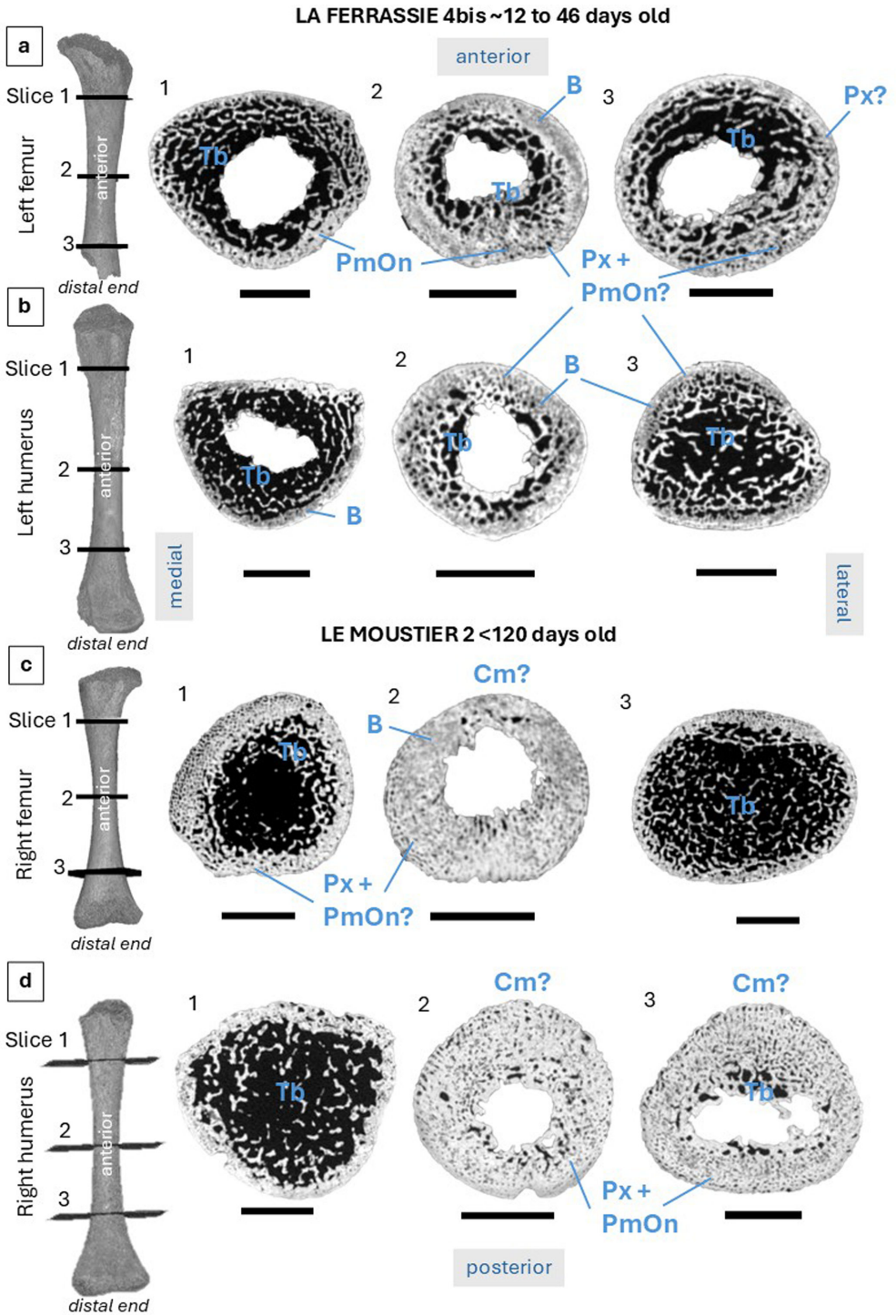

Figure 7. Bone microanatomy visualized in the micro-CT scans of the humerus and the femur in La Ferrassie 4bis (a,b) and Le Moustier 2 (c,d). Scale bars are 10 mm. Labels are in representative regions only indicating: bioerosion (B), plexiform-style bone (Px), primary osteons (PmOn), combination of Px and PmOn (Px + PmOn), trabeculae (Tb) and possible beginning of compaction (Cm?).

3.2. Deciduous teeth

The root of the Sesselfelsgrotte 2 tooth is almost fully resorbed (figures 8 and 9), while the Sesselfelsgrotte 3 tooth is very incomplete, with only approximately one-quarter of the crown preserved and the root also almost completely absent (figures 10 and 11). The anatomical identification as a deciduous lower left second molar is, thus, tentative. Visual inspection of the root appears to show resorption of three-quarters of its length (figure 10), but it is unclear if it may be broken and not resorbed.

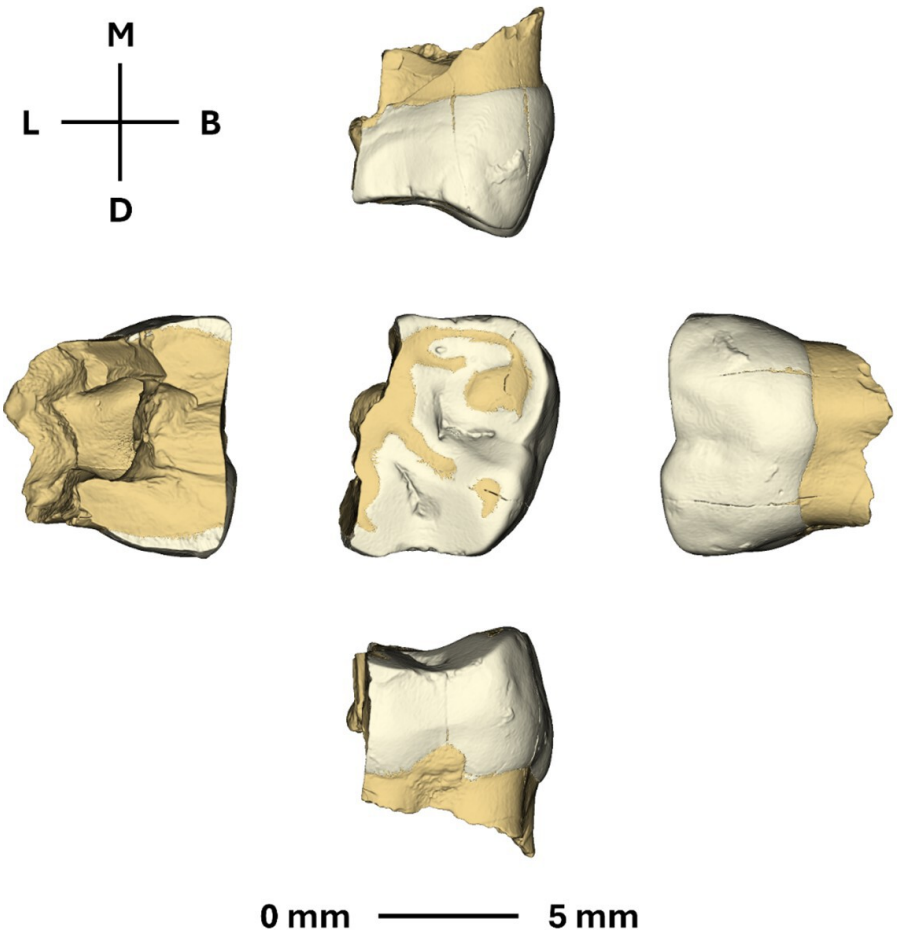

Figure 8. Sesselfelsgrotte 2 (upper left second deciduous molar). B: buccal, D: distal, L: lingual, M: mesial.

Although the Sessefelsgrotte 2 tooth is not fully preserved (part of the lingual half is absent), the tooth crown is worn with dentine exposure in the mesial-buccal cusp, less so in the distal-buccal cusp and, based on the preserved region, presumably more in the lingual half of the tooth (approximately dental wear stage 5 of the wear scale of Smith [99]). This, together with the root resorption and the wear preclude observation of the whole dentinal record. However, several hypodensities (areas of less mineralization) were detected in the primary coronal circumpulpal dentine. Specifically, three *foci* of reduced density were detected in the mesial and distal regions of the circumpulpal dentine away from the enamel dentine junction (and so from the mantle dentine in the crown; figure 9). These regions are visible as clusters of dark-grey/black pinpoints and/or larger black hole-like regions (figure 9). Although the tooth presents multiple internal fractures, these hypodensities are not present in the affected regions.

Sesselfelsgrotte 3 is incomplete, with extensive occlusal dental wear and a small enamel island remaining on the preserved occlusal surface (figure 10) (which suggests an approximate dental wear stage 6–7 on the scale of Smith [99] if this region is representative of the full occlusal surface). Similar to Sesselfelsgrotte 2, several hypodensities were detected within the primary coronal circumpulpal dentine. Specifically, a region of reduced density was detected in the circumpulpal dentine and distant from the enamel dentine junction (and so from the mantle dentine in the crown; figure 11) in which dark-grey/black pinpoints and/or larger black hole-like regions are found. Although the tooth presents multiple internal fractures, these hypodensities are not associated with the affected regions.

Neanderthal juvenile development has been studied using markers of disruption to dental growth and development as, unlike bones, teeth do not remodel. Various factors that are sufficiently severe may be macroscopically visible on tooth surfaces in the form of enamel hypoplasia (i.e. enamel surface defects such as pits, furrows and bands) [100,101]. High frequencies of dental enamel hypoplasia, which spans the juvenile growth period as enamel is forming in different teeth and capturing those defects, have been reported in Neanderthals, in some cases clustering within the range of modern human groups with high incidences of such defects [102–105]. A more recent study further examining

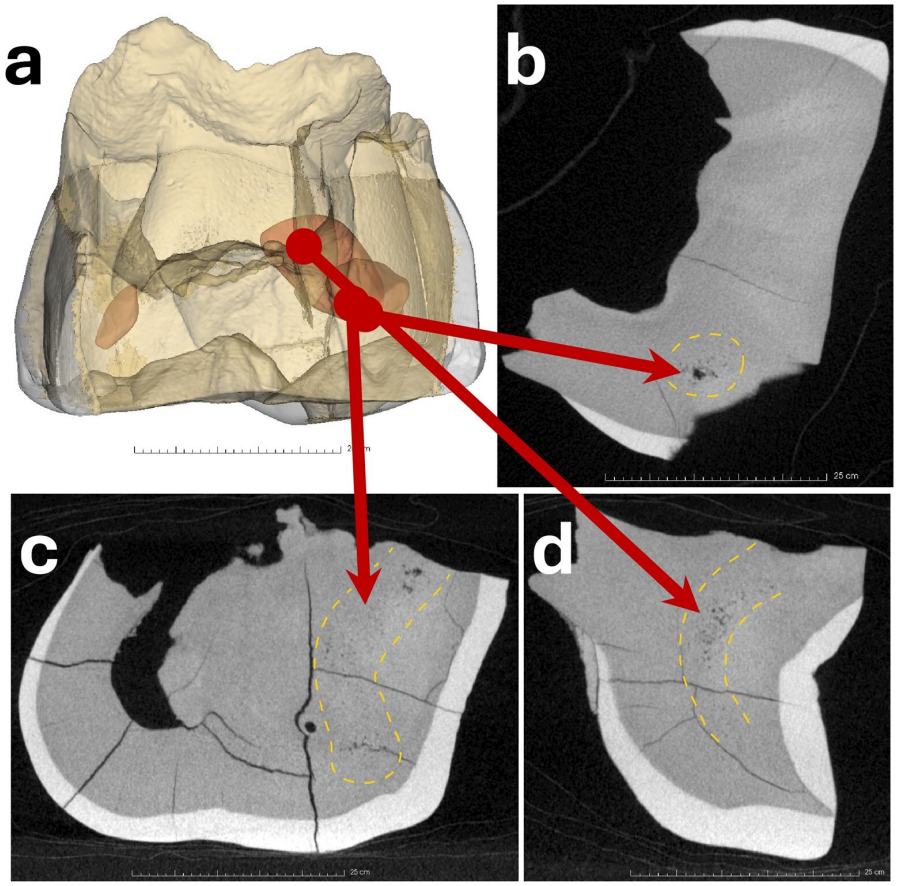

Figure 9. Sesselfelsgrotte 2: (a) Spatial distribution and examples of (b,c) hole-like or (c,d) pinpoint hypodensities in the crown circumpulpal dentine in the upper second deciduous molar from Sesselfelsgrotte. (d) shows a region where these hypodensities are clustered.

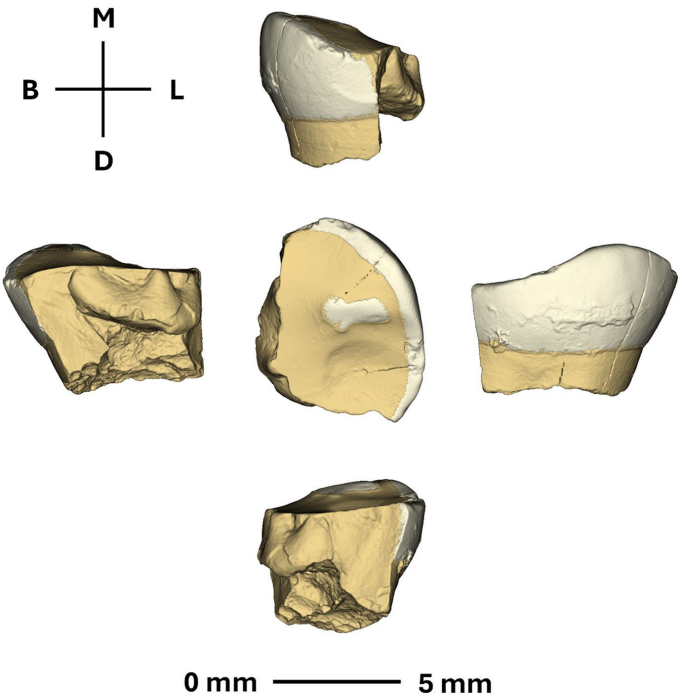

Figure 10. Sessefelsgrotte 3 (lower left second deciduous molar). B: buccal, D: distal, L: lingual, M: mesial.

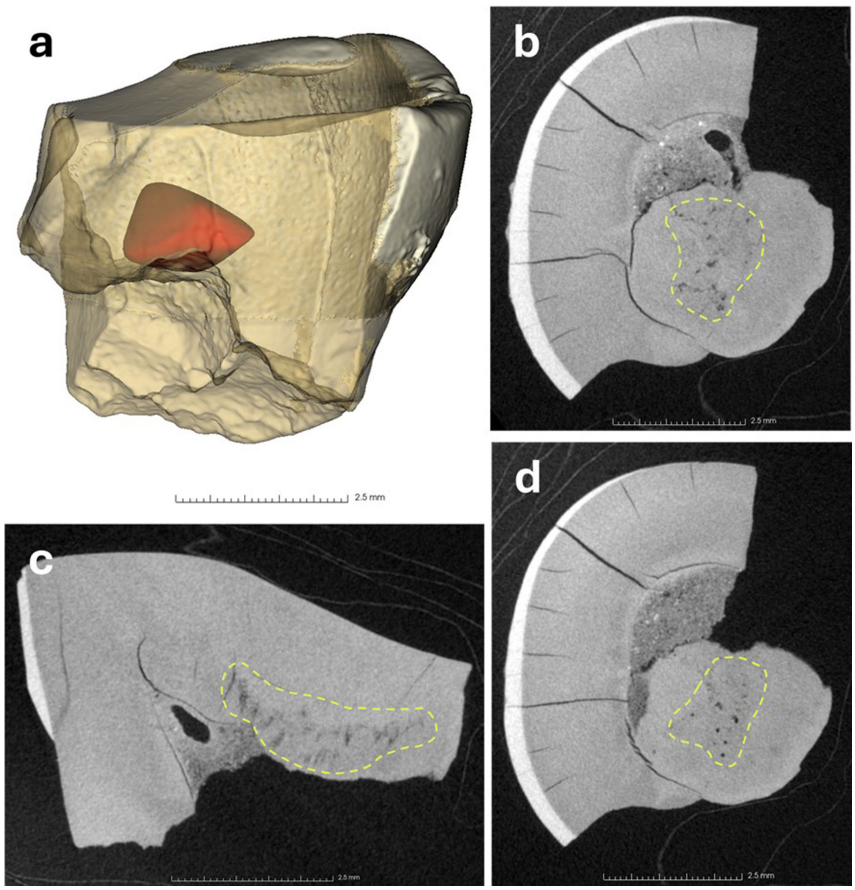

Figure 11. (a) Spatial distribution and (b–d) examples of hypodensities in the crown circumpulpal dentine in Sesselfelsgrotte 3.

such developmental disorders found comparable disturbance severity between Neanderthals and other modern human groups, despite Neanderthals having shallower hypoplasia (possibly due to faster tooth development) [106]. Moreover, despite Neanderthals and Upper Palaeolithic modern humans showing apparent comparable probabilities of developing hypoplasia, Neanderthals seem to form them at later ages than modern humans [102]. Other studies examining tooth developmental defects at a microscopic level report dentin mineralization defects [107,108]. While the early report of Sognnaes [107] related those inter-globular dentin defects to vitamin D deficiency, it has also been hypothesized they may be of developmental rather than pathological origin [108].

The hypodensities detected in both Sesselfelsgrotte 2 and 3 are consistent with the appearance of documented IGD in historical modern human teeth imaged with micro-CT [20,109]. It is impossible to definitively ascribe an underlying aetiology to IGD in fossil remains. The presence of IGD has been clinically associated with inborn errors of vitamin D metabolism [57,110]. Additionally, IGD has been noted in modern human archaeological individuals with macroscopic skeletal evidence of rickets or osteomalacia, probably due to nutritional vitamin D deficiency when the environmental context is considered [109,111,112]. However, any disorder that inhibits availability of calcium for the mineralization of hard tissues will produce a similar suite of skeletal lesions (rickets/osteomalacia) and this is probably true for IGD as well [113,114].

Because pathological IGD arises due to a systemic disturbance in pre-dentine mineralization, it occurs in both sides of the teeth in band-like formations along incremental growth lines and across several teeth [108]. There is some debate over how much IGD needs to be present in a region to be classified as 'pathological' as opposed to IGD that forms from the normal retraction of odontoblasts within dentine tubules (developmental IGD). However, developmental IGD should be present in the region most proximal to the dentine–enamel junction, rather than deeper in the primary dentine, and is not expected to form in discrete bands along incremental growth lines [111,115]. Additionally, comparison of ground histological sections and micro-CT data found that IGD typically scored as developmental is too small and widely spaced to be visualized on micro-CT scans [20]. Thus, the IGD in Sesselfelsgrotte 2 and 3 is probably abnormal and suggestive of a period of poor mineral

metabolism during growth. Potential causes include nutritional vitamin D deficiency and/or dietary calcium deficiency, a period of poor calcium absorption due to intestinal disease, or temporary renal compromise [113,116]. Because the severity and number of episodes of IGD in x-linked hypophosphatemic rickets is variable and we only have a partial development record, we cannot exclude this as a possibility [117].

Due to a lack of visibility of dentine incremental lines, it is not possible to identify the chronological age that the IGD occurred but based upon the duration of Neanderthal deciduous molar formation it is possible to suggest a range of biological ages when the poorly mineralized dentin may have formed. Upper second molar enamel of modern humans starts to form around three months before birth [118]. Dentine secretion is initially slightly in advance, and the crown is formed approximately 13 to 17 months after birth [118,119]. The Krapina Neanderthal deciduous first molar crowns formed over a slightly shorter postnatal period [21], which was probably due to the slightly accelerated rates of formation that have been reported for some Neanderthal deciduous [70] and permanent teeth [69,71]. Assuming that the dm2 of Sesselfelsgrotte 2 and 3 formed over a slightly shorter, or a period that was equivalent to modern human dm2's, then the IGD would occur somewhere between the third trimester and up to the middle of the second postnatal year. Most likely the period of poor mineralization occurred towards the middle and end of this period given the position of the IGD in figures 8 and 11.

Previous studies suggest that several aspects of Neanderthal femoral curvature and non-adult skull morphology were pathologically induced and specifically related to rickets/osteomalacia [120–123]. Despite those early interpretations, such Neanderthal morphological aspects have been dismissed as related to rickets/osteomalacia [122,124], and currently the earliest reported hypothesized cases of vitamin D deficiency originate from layer B of the Tabun cave, from which other dental remains have been dated to approximately 82–92 ka [125]. Specifically, one adolescent first molar and one left mandibular first molar from an individual with 6–12 years of age at death is said to show clear evidence of interglobular dentine [107]. Additionally, one maxillary left central incisor from a young adolescent displayed some granularity but no large regions of interglobular dentine [107]. Although these teeth are hypothesized to be Neanderthal [107], this tentative classification lacks confirmation [126]. Moreover, D'Ortenzio *et al.* [108] argue that these cases are probably of developmental origin, rather than induced by vitamin D deficiency. More recently, one undisputedly Neanderthal tooth from Lakonis, Greece, dated to 38–44 ka [127,128], was also reported to display interglobular dentine [129]. Thus, presently, reports of interglobular dentine in Neanderthals are restricted to the Lakonis individual [129] and to the tentative cases from Tabun [107]. The Sesselfelsgrotte 2 and 3 deciduous Neanderthal teeth add to these few reported possible vitamin D deficiency-induced IGD cases and are one of the earliest, if not the earliest. However, as mentioned above, IGD is a clinically common finding in modern humans and an evidenced-based threshold for the levels of serum vitamin D at which IGD begins to form have not yet been established. Vitamin D deficiency is a major health issue in modern times and the frequency at which it is found in clinical thin sections may or may not be related to the global prevalence of this condition. Work to explore the relationship between serum vitamin D status and IGD formation in modern human teeth is ongoing.

4. Conclusion

In this study, we examined bone microanatomy in the fossil bones of Sesselfelsgrotte 1 Neanderthal previously estimated to have died as a perinate, based on osteometry. Using non-invasive micro-CT, we found that all bones showed broad microanatomical patterns consistent with modern human fetal growth in the final trimester of pregnancy approaching eight–nine months, which agrees with the prior macroscopic measurements. We observed a combination of immature, probably woven, plexiform-like and isolated primary osteonal bone tissues which are typical for rapidly growing and fast forming skeletons. This is consistent with a younger Neanderthal than, for example, the 1.5–1.7-year-old Dederiyeh child bone histology specimens, which had secondary osteons. However, in the context of what is currently known for Neanderthal fetal and infant bone tissue growth, our study contributes a new perspective that their fetal growth might have had some acceleration in long bone formation despite the large consistency with modern humans until at least 1–2 years. Additionally, we have observed the potential earliest, approximately 75 ka, and clearest presence of interglobular dentine that is probably pathological in a Neanderthal lineage. Although we refrain from attributing a definitive cause for this lesion, it is indicative of poor mineral metabolism and is the earliest evidence of metabolic bone disease in a non-anatomically modern human to date.

Ethics. This work did not require ethical approval from a human subject or animal welfare committee.

Data accessibility. The fossils are permanently stored and curated at the Prehistoric and Protohistoric Museum of the UFG Institutes based at the Friedrich-Alexander-Universität (FAU) in Erlangen (Bavaria). The fossils are not currently displayed, to see the materials please contact Thorsten Uthmeier. The micro-CT scans of the specimens examined in this study are available open access from Morphosource: https://www.morphosource.org/organizations/000809898 [81]. Supplementary material is available online [130].

Declaration of AI use. We have not used AI-assisted technologies in creating this article.

Authors' contributions. J.J.M.: conceptualization, formal analysis, funding acquisition, investigation, methodology, project administration, validation, visualization, writing—original draft, writing—review and editing; R.M.G.: conceptualization, data curation, formal analysis, funding acquisition, investigation, methodology, project administration, resources, software, validation, visualization, writing—review and editing; A.M.S.-S.: formal analysis, investigation, methodology, validation, visualization, writing—review and editing; K.P.: investigation, methodology, validation, visualization, writing—review and editing; F.D.: data curation, investigation, methodology, resources, writing—review and editing; P.M.: formal analysis, investigation, methodology, validation, visualization, writing—review and editing; T.R.: data curation, investigation, resources, visualization, writing—review and editing; C.P.: formal analysis, investigation, methodology, resources, writing—review and editing; T.U.: data curation, methodology, resources, writing—review and editing; A.B.: conceptualization, data curation, formal analysis, funding acquisition, investigation, methodology, project administration, resources, validation, visualization, writing—review and editing.

All authors gave final approval for publication and agreed to be held accountable for the work performed therein.

Conflict of interest declaration. We declare we have no competing interests.

Funding. J.J.M. receives funding from the Australian Research Council (FT240100030). R.M.G. is funded by the Fundação para a Ciência e a Tecnologia (contract reference 2023.10993.TENURE.006; R&D project 'ParaFunction', reference 2022.07737.PTDC, https://doi.org/10.54499/2022.07737.PTDC). A.B. is funded by the Portuguese Ministry of Science (2002.08622.CEECIND) and has received funding for the analysis of Sesselfelsgrotte skeletal and dental remains by the National Geographic Society (NGS-96087R-22).

Acknowledgements. We thank Christina Kyriakouli and Gabriel Ferreira from Senckenberg Centre for Human Evolution and Palaeoenvironment for operating the micro-CT scanner at the University of Tübingen, Agnes Fatz for high resolution photographs of the skeletal and dental elements from Sesselfelsgrotte, Thomas Higham and Andreas Pfemeter for discussions about preliminary ^{14}C dating results, the Muséum National d'histoire Naturelle (Paris) for facilitating access to the micro-CT scans of La Ferrassie 4bis and Le Moustier 2, and two reviewers for their constructive feedback on an earlier version of our manuscript.

References

1. Mylopotamitaki D *et al*. 2024 *Homo sapiens* reached the higher latitudes of Europe by 45,000 years ago. *Nature* **626**, 341–346. (doi:10.1038/s41586-023-06923-7)
2. Guil-Guerrero JL, Manzano-Agugliaro F. 2023 Worldwide research trends on Neanderthals. *J. Quat. Sci.* **38**, 208–220. (doi:10.1002/jqs.3476)
3. Petr M *et al*. 2020 The evolutionary history of Neanderthal and Denisovan Y chromosomes. *Science* **369**, 1653–1656. (doi:10.1126/science.abb6460)
4. Peyrégne S, Slon V, Kelso J. 2024 More than a decade of genetic research on the Denisovans. *Nat. Rev. Genet.* **25**, 83–103. (doi:10.1038/s41576-023-00643-4)
5. Stringer C. 2025 Human evolution: the lonely Neanderthal? *Curr. Biol.* **35**, R29–R31. (doi:10.1016/j.cub.2024.11.043)
6. Stringer C, Crété L. 2022 Mapping interactions of *H. neanderthalensis* and *Homo sapiens* from the fossil and genetic records. *PaleoAnthropology* **2022**, 401–412. (doi:10.48738/2022.iss2.130)
7. Golovanova LV, Hoffecker JF, Kharitonov VM, Romanova GP. 1999 Mezmaiskaya cave: a Neanderthal occupation in the Northern Caucasus. *Curr. Anthropol.* **40**, 77–86. (doi:10.1086/515805)
8. Maureille B. 2002 La redécouverte du nouveau-né néandertalien Le Moustier 2. PALEO. *Revue d'archéologie Préhistorique* **14**, 221–238. (doi:10.4000/paleo.1458)
9. Maureille B. 2002 A lost Neanderthal neonate found. *Nature* **419**, 33–34. (doi:10.1038/419033a)
10. Maureille B. 2005 The rediscovery of Le Moustier 2 Neandertal specimen. In *The Neanderthal adolescent Le Moustier 1, new aspects, new results* (ed. H Ullrich), pp. 63–72. Berlin, Germany: Staalische Museen zu Berlin—Preußishcer Kulturbesitz.
11. Peyrony D. 1930 Le Moustier ses gisements, ses industries, ses couches géologiques. *Rev. D'Anthropologie* **40**, 48–76.
12. Rak Y, Kimbel WH, Hovers E. 1994 A Neandertal infant from Amud Cave, Israel. *J. Hum. Evol.* **26**, 313–324. (doi:10.1006/jhev.1994.1019)
13. Rathgeber T. 2006 Fossile Menschenreste aus der Sesselfelsgrotte im unteren Altmühltal (Bayern, Bundesrepublik Deutschland). *Quartär* **53**, 33–59.
14. Bastir M, O'Higgins P, Rosas A. 2007 Facial ontogeny in Neanderthals and modern humans. *Proc. R. Soc. B Biol. Sci.* **274**, 1125–1132. (doi:10.1098/rspb.2006.0448)
15. García-Martínez D *et al*. 2020 Early development of the Neanderthal ribcage reveals a different body shape at birth compared to modern humans. *Sci. Adv.* **6**, eabb4377. (doi:10.1126/sciadv.abb4377)

16. Gunz P, Neubauer S, Golovanova L, Doronichev V, Maureille B, Hublin JJ. 2012 A uniquely modern human pattern of endocranial development: insights from a new cranial reconstruction of the Neandertal newborn from Mezmaiskaya. *J. Hum. Evol.* **62**, 300–313. (doi:10.1016/j.jhevol.2011.11.013)
17. Ponce de León MS, Golovanova L, Doronichev V, Romanova G, Akazawa T, Kondo O, Ishida H, Zollikofer CPE. 2008 Neanderthal brain size at birth provides insights into the evolution of human life history. *Proc. Natl Acad. Sci. USA* **105**, 13764–13768. (doi:10.1073/pnas.0803917105)
18. Freund G. 1998 *Sesselfelsgrotte: I: Grabungsverlauf und Stratigraphie*. Saarbrücken, Germany: Saarbrucker Druckerei und Verlag.
19. Richter D, Mauz B, Böhner U, Weismüller W, Wagner GA, Freund G, Rink WJ, Richter J. 2000 Luminescence dating of the Middle/Upper Palaeolithic sites 'Sesselfelsgrotte' and 'Abri I Schulerloch', Altmühltal, Bavaria. In *Neanderthals and modern humans – discussing the transition: central and eastern Europe from 50.000–30.000 b.p* (eds J Orschiedt, C Weniger), pp. 30–41, vol. 2. Mettmann, Germany: Wissenschaftliche Schriften des Neanderthal Museums.
20. Colombo A, D'Ortenzio L, Bertrand B, Coqueugniot H, Knüsel CJ, Kahlon B, Brickley M. 2019 Micro-computed tomography of teeth as an alternative way to detect and analyse vitamin D deficiency. *J. Archaeol. Sci.* **23**, 390–395. (doi:10.1016/j.jasrep.2018.11.006)
21. Mahoney P *et al*. 2021 Growth of Neanderthal infants from Krapina (120–130 ka), Croatia. *Proc. R. Soc. B* **288**, 20212079. (doi:10.1098/rspb.2021.2079)
22. Nava A *et al*. 2020 Early life of Neanderthals. *Proc. Natl Acad. Sci. USA* **117**, 28719–28726. (doi:10.1073/pnas.2011765117)
23. Sawada J, Kondo O, Nara T, Dodo Y, Akazawa T. 2004 Bone histomorphology of the Dederiyeh Neanderthal child. *Anthropol. Sci.* **112**, 247–256. (doi:10.1537/ase.00094)
24. Cunningham C, Scheuer L, Black S. 2016 *Developmental juvenile osteology*. San Diego, CA: Academic Press.
25. Gardner E, Gray DJ. 1970 The prenatal development of the human femur. *Am. J. Anat.* **129**, 121–140. (doi:10.1002/aja.1001290202)
26. Land C, Schoenau E. 2008 Fetal and postnatal bone development: reviewing the role of mechanical stimuli and nutrition. *Best Pract. Res. Clin. Endocrinol. Metab.* **22**, 107–118. (doi:10.1016/j.beem.2007.09.005)
27. Nemec U, Nemec SF, Krakow D, Brugger PC, Malinger G, Graham JM, Rimoin DL, Prayer D. 2011 The skeleton and musculature on foetal MRI. *Insights Imaging* **2**, 309–318. (doi:10.1007/s13244-011-0075-6)
28. Salle BL, Rauch F, Travers R, Bouvier R, Glorieux FH. 2002 Human fetal bone development: histomorphometric evaluation of the proximal femoral metaphysis. *Bone* **30**, 823–828. (doi:10.1016/s8756-3282(02)00724-x)
29. Scheuer L, Black S. 2004 *The juvenile skeleton*. London, UK: Elsevier.
30. Thomson AM. 1951 Human foetal growth. *Br. J. Nutr.* **5**, 158–166. (doi:10.1079/bjn19510019)
31. Weaver CM, Fuchs RK. 2014 Skeletal growth and development. In *Basic and applied bone biology* (eds DB Burr, MR Allen), pp. 245–260. San Diego, CA, USA: Academic Press. (doi:10.1016/B978-0-12-416015-6.00012-5)
32. Moreno MM, Doe DM, González NC, Martínez DG, Martín AG, Cambra-Moo O. 2025 Revealing developmental transitions in perinatal and infant individuals through microanatomical analysis. *Am. J. Hum. Biol.* **37**, e70101. (doi:10.1002/ajhb.70101)
33. Johansen JS, Høyer PE, Larsen LA, Price PA, Møllgård K. 2007 YKL-40 protein expression in the early developing human musculoskeletal system. *J. Histochem. Cytochem.* **55**, 1213–1228. (doi:10.1369/jhc.7A7245.2007)
34. Chamley CA. 2005 The musculoskeletal system. In *Developmental anatomy and physiology of children* (eds CA Chamley, P Carson, D Randall, M Sandwell), pp. 59–95. London, UK: Elsevier Churchill Livingstone.
35. White A, Wallis G. 2001 Endochondral ossification: a delicate balance between growth and mineralisation. *Curr. Biol.* **11**, R589–R591. (doi:10.1016/s0960-9822(01)00359-1)
36. Glorieux FH, Salle BL, Travers R, Audra PH. 1991 Dynamic histomorphometric evaluation of human fetal bone formation. *Bone* **12**, 377–381. (doi:10.1016/8756-3282(91)90025-E)
37. Burton P, Nyssen-Behets C, Dhem A. 1989 Haversian bone remodelling in human fetus. *Acta Anat.* **135**, 171–175. (doi:10.1159/000146748)
38. Verbruggen SW, Kainz B, Shelmerdine SC, Hajnal JV, Rutherford MA, Arthurs OJ, Phillips ATM, Nowlan NC. 2018 Stresses and strains on the human fetal skeleton during development. *J. R. Soc. Interface* **15**, 20170593. (doi:10.1098/rsif.2017.0593)
39. Ernst LM, Ruchelli ED, Huff DS. 2011 *Color atlas of fetal and neonatal histology*. New York, NY: Springer.
40. Filipowska J, Tomaszewski KA, Niedźwiedzki Ł, Walocha JA, Niedźwiedzki T. 2017 The role of vasculature in bone development, regeneration and proper systemic functioning. *Angiogenesis* **20**, 291–302. (doi:10.1007/s10456-017-9541-1)
41. Shapiro F, Wu JY. 2019 Woven bone overview: structural classification based on its integral role in developmental, repair and pathological bone formation throughout vertebrate groups. *Eur. Cells Mater. J.* **38**, 137–167. (doi:10.22203/eCM.v038a11)
42. Dhawan V, Kapoor K, Sharma M, Singh B, Sehgal A, Kochhar S. 2014 Histological study of the developing human femur. *Eur. J. Anat.* **18**, 273–282.
43. Booth TJ, Redfern RC, Gowland RL. 2016 Immaculate conceptions: micro-CT analysis of diagenesis in Romano-British infant skeletons. *J. Archaeol. Sci.* **74**, 124–134. (doi:10.1016/j.jas.2016.08.007)
44. Chu TW, Shannon P, Parks T. 2024 Skeletal growth arrest lines in fetal remains: histopathology and correlative placental pathology. *Pediatr. Dev. Pathol.* **27**, 23–31. (doi:10.1177/10935266231195750)
45. Eleazer CD. 2007 Age-related histomorphometric changes in human fetal long bones. Masters Thesis, [Knoxville, TN, USA]: University of Tennessee.
46. Caccia G, Magli F, Tagi VM, Porta DGA, Cummaudo M, Márquez-Grant N, Cattaneo C. 2016 Histological determination of the human origin from dry bone: a cautionary note for subadults. *Int. J. Legal Med.* **130**, 299–307. (doi:10.1007/s00414-015-1271-6)

47. Goldman HM, Mcfarlin SC, Cooper DML, Thomas CDL, Clement JG. 2009 Ontogenetic patterning of cortical bone microstructure and geometry at the human mid-shaft femur. *Anat. Rec.* **292**, 48–64. (doi:10.1002/ar.20778)
48. Pfeiffer S. 2006 Cortical bone histology in juveniles. *Doc. Archaeobiologiae* **4**, 15–28.
49. Baltadjiev G. 1995 Micromorphometric characteristics of osteons in compact bone of growing tibiae of human fetuses. *Acta Anat.* **154**, 181–185. (doi:10.1159/000147767)
50. Schoenwolf GC, Bleyl SB, Brauer PR, Francis-West PH. 2014 *Larsen's human embryology*. Philadelphia, PA, USA: Elsevier Health Sciences.
51. Hillson S. 1996 *Dental anthropology*. Cambridge, UK: Cambridge University Press.
52. AlQahtani SJ, Hector MP, Liversidge HM. 2010 Brief communication: the London atlas of human tooth development and eruption. *Am. J. Phys. Anthropol.* **142**, 481–490. (doi:10.1002/ajpa.21258)
53. Scheuer L, Black S. 2000 *Developmental junvenile osteology*. San Diego, CA, USA: Elsevier Academic Press. (doi:10.1016/B978-012624000-9/50004-6)
54. Liversidge HM, Molleson T. 2018 Human tooth development, tooth length and eruption; a study of British archaeological dentitions. *Hist. Biol.* **30**, 166–173. (doi:10.1080/08912963.2017.1305375)
55. Ireland R. 2010 *A dictionary of dentistry*. Oxford, UK: Oxford University Press.
56. Abe K, Ooshima T, Lily TSM, Yasufuku Y, Sobue S. 1988 Structural deformities of deciduous teeth in patients with hypophosphatemic vitamin D-resistant rickets. *Oral Surg. Oral Med. Oral Pathol.* **65**, 191–198. (doi:10.1016/0030-4220(88)90165-x)
57. Seow WK, Romaniuk K, Sclavos S. 1989 Micromorphologic features of dentin in vitamin D-resistant rickets: correlation with clinical grading of severity. *Pediatr. Dent.* **11**, 203–208.
58. Schoenwolf GC, Bleyl SB, Brauer PR, Francis-West PH. 2014 *Larsen's human embryology*. Philadelphia, TN, USA: Elsevier Health Sciences.
59. Harris EF. 2015 Odontogenesis. In *A companion to dental anthropology* (eds JD Irish, GR Scott), pp. 142–158. Hoboken, NJ: Wiley.
60. Sasaki C. 2003 Age determination of the Dederiyeh 1 Neanderthal child using enamel cross-striations. In *Neanderthal burials, excavations of the Dederiyeh Cave, Afrin, Syria* (eds T Akazawa, S Muhesen), pp. 263–267. Kyoto, Japan: International Research Center for Japanese Studies.
61. Been E, Hovers E, Rak Y, Le Cabec A, Dean C, Barash A. 2026 Rapid growth in a Neandertal infant from Amud Cave in Israel. *Curr. Biol.* **36**, 2434–2441. (doi:10.1016/j.cub.2026.03.054)
62. Chevalier T, Colard T, Colombo A, Golovanova L, Doronichev V, Hublin JJ. 2021 Early ontogeny of humeral trabecular bone in Neandertals and recent modern humans. *J. Hum. Evol.* **154**, 102968. (doi:10.1016/j.jhevol.2021.102968)
63. Heim JL. 1976 *Les Hommes Fossiles de la Ferrassie. Le gisement. Les squelettes adultes (crâne et squelette du tronc)*. vol. 1. Paris, France: Masson: Archives de l'Institut de Paléontologie Humaine.
64. Heim JL. 1982 *Les enfants néandertaliens de La Ferrassie: étude anthropologique et analyse ontogénique des hommes de Néandertal*. Paris, France: FondationSinger-Polignac.
65. Heim JL. 1982 *Les hommes fossiles de la ferrassie. ii. les squelettes d'Adultes: squelettes des membres*. Paris, France: Masson.
66. Freidline SE, Gunz P, Harvati K, Hublin JJ. 2013 Evaluating developmental shape changes in *Homo antecessor* subadult facial morphology. *J. Hum. Evol.* **65**, 404–423. (doi:10.1016/j.jhevol.2013.07.012)
67. Lacruz RS *et al*. 2015 Ontogeny of the maxilla in Neanderthals and their ancestors. *Nat. Commun.* **6**, 1–6. (doi:10.1038/ncomms9996)
68. Guatelli-Steinberg D, Reid DJ, Bishop TA, Larsen CS. 2005 Anterior tooth growth periods in Neandertals were comparable to those of modern humans. *Proc. Natl Acad. Sci. USA* **102**, 14197–14202. (doi:10.1073/pnas.0503108102)
69. Ramirez Rozzi FV, Bermudez de Castro JM. 2004 Surprisingly rapid growth in Neanderthals. *Nature* **428**, 936–939. (doi:10.1038/nature02428)
70. Macchiarelli R, Bondioli L, Debénath A, Mazurier A, Tournepiche JF, Birch W, Dean MC. 2006 How Neanderthal molar teeth grew. *Nature* **444**, 748–751. (doi:10.1038/nature05314)
71. Smith TM *et al*. 2010 Dental evidence for ontogenetic differences between modern humans and Neanderthals. *Proc. Natl Acad. Sci. USA* **107**, 20923–20928. (doi:10.1073/pnas.1010906107)
72. Smith TM, Toussaint M, Reid DJ, Olejniczak AJ, Hublin JJ. 2007 Rapid dental development in a Middle Paleolithic Belgian Neanderthal. *Proc. Natl Acad. Sci. USA* **104**, 20220–20225. (doi:10.1073/pnas.0707051104)
73. Barbieri A, Maier A, Lauer T, Mischka C, Hattermann M, Uthmeier T. 2022 Post-LGM environments and foragers on the move: new data from the lower Altmühl Valley (Franconian Jura, SE Germany). *J. Hum. Evol.* **173**, 103267. (doi:10.1016/j.jhevol.2022.103267)
74. Birkner F. 1936 Ur-und Vorgeschichte Bayerns. *Nachrichten Aus Niedersachsens Urgesch.* **10**, 101.
75. Böhner U. 2008 Die Schicht E3 der Sesselfelsgrotte und die Funde aus dem Abri I am Schulerloch. Späte Micoquien-Inventare und ihre Stellung zum Moustérien. Stuttgart, Germany: Franz Steiner Verlag.
76. Obermaier H, Wernert P. 1914 Paläolithbeiträge aus Nordbayern. *Mitt. Anthropol. Ges. Wien* **14**, 44–62.
77. Street M, Terberger T, Orschiedt J. 2006 A critical review of the German Paleolithic hominin record. *J. Hum. Evol.* **51**, 551–579. (doi:10.1016/j.jhevol.2006.04.014)
78. Richter J. 2001 For lack of a wise old man? Late Neanderthal land use patterns in the Altmühl River Valley, Southern Germany. In *Middle stone age and middle palaeolithic settlement patterns* (ed. NJ Conard), pp. 205–220. Köln, Germany: Universität zu Köln Institut für Ur- und Frühgeschichte.
79. Fotiadou CM *et al*. 2026 Archaeogenetic insights into the demographic history of Late Neanderthals. *Proc. Natl Acad. Sci. USA* **123**, e2520565123. (doi:10.1073/pnas.2520565123)
80. Abella J, Martín-Perea DM, Valenciano A, Hontecillas D, Montoya P, Morales J. 2021 Coprolites in natural traps: direct evidence of bone-eating carnivorans from the Late Miocene Batallones-3 site, Madrid, Spain. *Lethaia* **54**, 762–774. (doi:10.1111/let.12438)

81. Godinho RM. 2026 *ICArEHB:Sesselfelsgrotte*. Morphosource. See https://www.morphosource.org/organizations/000809898.
82. Fedorov A *et al*. 2012 3D Slicer as an image computing platform for the Quantitative Imaging Network. *Magn. Reson. Imaging* **30**, 1323–1341. (doi:10.1016/j.mri.2012.05.001)
83. Mandl K, Carlson KSD, Brönnimann D, McCall A, Grassberger M, Teschler-Nicola M, Weiss-Krejci E, Metscher B. 2022 Substantiating microCT for diagnosing bioerosion in archaeological bone using a new Virtual Histological Index (VHI). *Archaeol. Anthropol. Sci.* **14**, 104. (doi:10.1007/s12520-022-01563-w)
84. Pitfield R, Miszkiewicz JJ, Mahoney P. 2017 Cortical histomorphometry of the human humerus during ontogeny. *Calcif. Tissue Int.* **101**, 148–158. (doi:10.1007/s00223-017-0268-1)
85. Su XW, Feng QL, Cui FZ, Zhu XD. 1997 Microstructure and micromechanical properties of the mid-diaphyses of human fetal femurs. *Connect. Tissue Res.* **36**, 271–286. (doi:10.3109/03008209709160227)
86. Valladas H, Geneste JM, Joron JL, Chadelle JP. 1986 Thermoluminescence dating of Le Moustier (Dordogne, France). *Nature* **322**, 452–454. (doi:10.1038/322452a0)
87. Guérin G *et al*. 2015 A multi-method luminescence dating of the Palaeolithic sequence of La Ferrassie based on new excavations adjacent to the La Ferrassie 1 and 2 skeletons. *J. Archaeol. Sci.* **58**, 147–166. (doi:10.1016/j.jas.2015.01.019)
88. Guérin G *et al*. 2023 A third Neanderthal individual from La Ferrassie dated to the end of the Middle Palaeolithic. *PaleoAnthropology* **23**, 22–28. (doi:10.48738/2023.iss1.811)
89. Martin RB, Burr DB. 1989 *Structure, function, and adaptation of compact bone*. New York, NY, USA: Raven Press.
90. Churchill SE. 2014 *Thin on the ground [electronic resource]: Neandertal biology, archeology and ecology*. Hoboken, NJ, USA: Wiley-Blackwell.
91. Pomeroy E. 2023 The different adaptive trajectories in Neanderthals and *Homo sapiens* and their implications for contemporary human physiological variation. *Comp. Biochem. Physiol. A Mol. Integr. Physiol.* **280**, 111420. (doi:10.1016/j.cbpa.2023.111420)
92. Goodfellow LR, Earl S, Cooper C, Harvey NC. 2010 Maternal diet, behaviour and offspring skeletal health. *Int. J. Environ. Res. Public Health* **7**, 1760–1772. (doi:10.3390/ijerph7041760)
93. Nowlan NC. 2015 Biomechanics of foetal movement. *Eur. Cells Mater.* **29**, 1–21. (doi:10.22203/eCM.v029a01)
94. Weaver TD, Hublin JJ. 2009 Neandertal birth canal shape and the evolution of human childbirth. *Proc. Natl Acad. Sci. USA* **106**, 8151–8156. (doi:10.1073/pnas.0812554106)
95. Hall A, Sherlock E, Sykes D. 2015 Does micro-CT scanning damage DNA in museum specimens? *J. Nat. Sci. Collections* **2**, 22–28.
96. Immel A *et al*. 2016 Effect of X-ray irradiation on ancient DNA in sub-fossil bones – guidelines for safe X-ray imaging. *Sci. Rep.* **6**, 32969. (doi:10.1038/srep32969)
97. Duval M, Martín-Francés L, Wood R. 2025 On the impact of micro-CT scanning on radiocarbon dating of fossil material: a cautionary note for the palaeoanthropological community and beyond. *Radiocarbon* **67**, 709–718. (doi:10.1017/rdc.2025.23)
98. Booth TJ. 2016 An Investigation Into the relationship between funerary treatment and bacterial bioerosion in European archaeological human bone. *Archaeometry* **58**, 484–499. (doi:10.1111/arcm.12190)
99. Smith BH. 1984 Patterns of molar wear in hunter–gatherers and agriculturalists. *Am. J. Phys. Anthropol* **63**, 39–56. (doi:10.1002/ajpa.1330630107)
100. Collignon AM, Vergnes JN, Germa A, Azogui S, Breinig S, Hollande C, Bonnet AL, Nabet C. 2022 Factors and mechanisms involved in acquired developmental defects of enamel: a scoping review. *Front. Pediatr.* **10**, 2022. (doi:10.3389/fped.2022.836708)
101. Goodman AH, Rose JC. 1990 Assessment of systemic physiological perturbations from dental enamel hypoplasias and associated histological structures. *Am. J. Phys. Anthropol.* **33**, 59–110. (doi:10.1002/ajpa.1330330506)
102. Guatelli-Steinberg D, Larsen CS, Hutchinson DL. 2004 Prevalence and the duration of linear enamel hypoplasia: a comparative study of Neandertals and Inuit foragers. *J. Hum. Evol.* **47**, 65–84. (doi:10.1016/j.jhevol.2004.05.004)
103. Hutchinson DL, Larsen CS, Choi I. 1997 Stressed to the max? Physiological perturbation in the Krapina Neandertals. *Curr. Anthropol.* **38**, 904–914. (doi:10.1086/204681)
104. Molnar S, Molnar IM. 1985 The incidence of enamel hypoplasia among the Krapina Neandertals. *Am. Anthropol.* **87**, 536–549. (doi:10.1525/aa.1985.87.3.02a00020)
105. Ogilvie MD, Curran BK, Trinkaus E. 1989 Incidence and patterning of dental enamel hypoplasia among the Neandertals. *Am. J. Phys. Anthropol.* **79**, 25–41. (doi:10.1002/ajpa.1330790104)
106. McGrath K, Limmer LS, Lockey AL, Guatelli-Steinberg D, Reid DJ, Witzel C, Bocaege E, McFarlin SC, El Zaatari S. 2021 3D enamel profilometry reveals faster growth but similar stress severity in Neanderthal versus *Homo sapiens* teeth. *Sci. Rep.* **11**, 522. (doi:10.1038/s41598-020-80148-w)
107. Sognnaes RF. 1956 Histologic evidence of developmental lesions in teeth originating from paleolithic, prehistoric, and ancient man. *Am. J. Pathol.* **32**, 547–577.
108. D'Ortenzio L, Kahlon B, Peacock T, Salahuddin H, Brickley M. 2018 The rachitic tooth: refining the use of interglobular dentine in diagnosing vitamin D deficiency. *Int. J. Paleopathol.* **22**, 101–108. (doi:10.1016/j.ijpp.2018.07.001)
109. Veselka B, Brickley MB, D'Ortenzio L, Kahlon B, Hoogland MLP, Waters-Rist AL. 2019 Micro-CT assessment of dental mineralization defects indicative of vitamin D deficiency in two 17th-19th century Dutch communities. *Am. J. Phys. Anthropol.* **169**, 122–131. (doi:10.1002/ajpa.23819)
110. Karemore T, Motwani M, Karemore V. 2022 Vitamin D deficiency and its effects on enamel, dentin, and pulp: a literature review. *J. Dent. Res. Rev.* **9**, 202–205. (doi:10.4103/jdrr.jdrr_69_22)

111. D'Ortenzio L, Ribot I, Raguin E, Schattmann A, Bertrand B, Kahlon B, Brickley M. 2016 The rachitic tooth: a histological examination. *J. Archaeol. Sci.* **74**, 152–163. (doi:10.1016/j.jas.2016.06.006)
112. Snoddy AME, Shaw H, Newman S, Miszkiewicz JJ, Stewart NA, Jakob T, Buckley H, Caffell A, Gowland R. 2024 Vitamin D status in post-medieval Northern England: insights from dental histology and enamel peptide analysis at Coach Lane, North Shields (AD 1711-1857). *PLoS One* **19**, e0296203. (doi:10.1371/journal.pone.0296203)
113. Vautour L, Goltzman D. 2018 Regulation of calcium homeostasis. In *Primer on the metabolic bone diseases and disorders of mineral metabolism* (ed. JP Bilezikian), pp. 163–172. Hoboken, NJ, USA: John Wiley & Sons. (doi:10.1002/9781119266594)
114. Vlok M, Snoddy AME, Ramesh N, Wheeler BJ, Standen VG, Arriaza BT. 2023 The role of dietary calcium in the etiology of childhood rickets in the past and the present. *Am. J. Hum. Biol.* **35**, e23819. (doi:10.1002/ajhb.23819)
115. Nanci A. 1994 *Ten Cate's oral histology: development, structure, and function*. St Louis, MO, USA: Elsevier.
116. Bikle D, S. Adams J, Christakos S. 2019 Vitamin D: production, metabolism, mechanism of action, and clinical requirements. In *Primer on the metabolic bone diseases and disorders of mineral metabolism* (ed. CJ Rosen), pp. 231–251, 9th edn. Hoboken, NJ, USA: John Wiley & Sons. (doi:10.1002/9781118453926)
117. Boukpessi T, Septier D, Bagga S, Garabedian M, Goldberg M, Chaussain-Miller C. 2006 Dentin alteration of deciduous teeth in human hypophosphatemic rickets. *Calcif. Tissue Int.* **79**, 294–300. (doi:10.1007/s00223-006-0182-4)
118. Mahoney P *et al*. 2025 Variation in modern human deciduous molar enamel formation time. *Am. J. Biol. Anthropol.* **188**, e70156. (doi:10.1002/ajpa.70156)
119. Sunderland EP, Smith CJ, Sunderland R. 1987 A histological study of the chronology of initial mineralization in the human deciduous dentition. *Arch. Oral Biol.* **32**, 167–174. (doi:10.1016/0003-9969(87)90130-0)
120. Czarnetzki A. 2000 The significance of pathological changes for judging the morphology of classical Neanderthals. In *Neanderthals and modern humans–discussing the transition: Central and Eastern Europe from 50.000–30.000 bp* (eds J Orschiedt, GC Weniger), pp. 296–302. Mettmann, Germany: Neanderthal Museum.
121. Ivanhoe F. 1970 Was Virchow right about Neandertal? *Nature* **227**, 577–579. (doi:10.1038/227577a0)
122. Ivanhoe F, Trinkaus E. 1983 On cranial deformation in Shanidar 1 and 5. *Curr. Anthropol.* **24**, 127–128. (doi:10.1086/202956)
123. Klaatsch HAL. 1901 Das Gliedmassenskelett des Neanderthalmenschen. *Anat. Anz.* **19**, 121–154.
124. De Groote I. 2011 Femoral curvature in Neanderthals and modern humans: a 3D geometric morphometric analysis. *J. Hum. Evol.* **60**, 540–548. (doi:10.1016/j.jhevol.2010.09.009)
125. Coppa A, Grün R, Stringer C, Eggins S, Vargiu R. 2005 Newly recognized Pleistocene human teeth from Tabun Cave, Israel. *J. Hum. Evol.* **49**, 301–315. (doi:10.1016/j.jhevol.2005.04.005)
126. Brickley MB, D'Ortenzio L, Kahlon B, Schattmann A, Ribot I, Raguin E, Bertrand B. 2017 Ancient Vitamin D deficiency: long-term trends. *Curr. Anthropol.* **58**, 420–427. (doi:10.1086/691683)
127. Harvati K, Panagopoulou E, Karkanas P. 2003 First Neanderthal remains from Greece: the evidence from Lakonis. *J. Hum. Evol.* **45**, 465–473. (doi:10.1016/j.jhevol.2003.09.005)
128. Panagopoulou E, Karkanas P, Tsartsidou G, Kotjabopoulou E, Harvati K, Ntinou M. 2002 Late pleistocene archaeological and fossil human evidence from Lakonis Cave, Southern Greece. *J. Field Archaeol.* **29**, 323–349. (doi:10.2307/3250896)
129. Smith TM, Harvati K, Olejniczak AJ, Reid DJ, Hublin JJ, Panagopoulou E. 2009 Brief communication: dental development and enamel thickness in the Lakonis Neanderthal molar. *Am. J. Phys. Anthropol.* **138**, 112–118. (doi:10.1002/ajpa.20898)
130. Miszkiewicz JJ, Godinho RM, Sohler-Snoddy AM, Pasda K, Detroit F, Mahoney P *et al*. 2026 Supplementary material from: Early development of Neanderthals revealed through virtual microanatomy (doi:10.6084/m9.figshare.c.8517014)